4. Results and Discussion

Bioactive compounds found in medicinal plants serve a crucial role in both traditional and modern medicine for treating various health conditions (Rathor, 2021). People have used medicinal plants for centuries in different cultural settings because it provides therapeutic benefits such as anti-inflammatory properties together with antioxidant, antimicrobial and anti-cancer activities. Active plant compounds including alkaloids, flavonoids, phenol and terpenoids compounds present in these plants maintain essential roles in promoting health and preventing diseases (Roy *et al.*, 2022).

This division displays the results and discussion to prove the anti-cancer efficacy of *Rhododendron arboreum* Sm. against Gastric Cancer.

4.1. Qualitative Phytochemical Analysis

Plants contain phytochemicals as chemical constituents which are responsible for therapeutic activity against various human diseases (Santhiravel *et al.*, 2022). Multiple phytochemical observations of *R. arboreum*

leaf and flower extracts confirmed the presence of different primary and secondary metabolites including alkaloids, flavonoids, phytosterols, phenols, tannins, diterpenes, proteins, amino acids, carbohydrates, saponins, quinones, coumarins, acidic compounds, catechins, volatile oils, resins, starch, carotenoids, oxalates and vitamin C (Table. 3 & 4). The methanol extracts of *R. arboreum* leaf and flower showed higher composition of phytoconstituents, this could be because of its polar characteristics, solubility and chemical stability, which makes it a highly effective extractive solvent (Kumar *et al.*, 2023). The methanol leaf extract contained high concentrations of alkaloids along with flavonoids, phytosterols, diterpene etc. While the flower extract contained major components of flavonoids, phytosterols, phenols, tannin etc. Saponins were detected only in leaves and flower extracts through chloroform-derived solutions and aqueous solutions respectively.

Different types of phytochemicals were identified in the present study using different solvent extracts, where methanol proved to be the most efficient extraction which confirms its capability to capture a wide range of bioactive compounds (Table. 3 & 4). The synthesis of natural metabolites is influenced by the plant's growing environment and solvent used for the extraction because both the factors determine phytochemical distribution in plants (Kumar *et al.*, 2023; Singh *et al.*, 2021). A study by Madhvi *et al.*, (2020) confirmed that ethanol and acetone (1:1) extraction of *Rhododendron* leaf contain abundant flavonoids and tannins, which correlates with present observation. The different bioactive compounds detected in the *R. arboreum* demonstrate potential therapeutic values of this plant.

The higher solubility of compounds in methanol solvent lead to higher yields of flavonoids and phenolic compounds compared to other solvents, thereby expanding the extraction of bioactive compounds that possess various pharmacological activities. The previous studies have proven that plant pharmaceutical properties depend on the phytoconstituents that are present in the plants (Tungmunnithum *et al.*, 2018). Therefore, it is also important to investigate solvent choice in phytochemical testing for proposing additional therapeutic potentials from *R. arboreum* (Kumar *et al.*, 2020).

Rawat *et al.*, (2016) performed qualitative analysis on *R. arboreum* leaf methanol extract to determine phytosterols together with flavonoids, phenols, alkaloids, carbohydrates, glycosides, sterols, steroids, terpenoids and tannins. Similar to present study, absence of saponin was detected in the *R. arboreum* leaf and flower extracts, except chloroform and aqueous extracts (Table. 3 & 4). The distribution of distinct phytochemicals varies due to the combination of extract type along with solvent and sample analysis technique. Similarly, Ahmad *et al.*, (2020) discovered that *R. arboreum* leaves processed with methanol possess anthraquinones and flavonoids in addition to terpenoids, steroids and tannins.

Table 3. Qualitative Analysis of Primary and Secondary Metabolites Present in *R. arboreum* Leaf Extracts

S.No	Test	Petroleum Ether	Chloroform	Acetone	Ethanol	Methanol	Aqueous
1.	Alkaloids	+	+	+	+	++	++
2.	Flavonoids	-	-	-	+	++	+
3.	Phytosterols	-	-	-	+	++	+
4.	Phenols	-	-	+	+	+	-
5.	Tannins	-	-	+	+	+	-
6.	Diterpenes	-	-	+	++	++	+
7.	Proteins	+	-	+	++	++	+
8.	Amino acids	-	-	-	+	++	+
9.	Carbohydrates	-	+	+	++	++	+
10.	Saponins	-	+	-	-	-	-
11.	Quinones	-	-	-	+	+	-
12.	Coumarins	+	-	+	+	++	-
13.	Acidic compounds	+	-	+	+	+	-
14.	Catechins	+	+	+	-	+	-
15.	Volatile oils	+	-	-	-	+	-
16.	Resin	-	+	+	+	+	-
17.	Starch	-	+	+	+	+	-
18.	Carotenoids	-	-	+	+	+	-
19.	Oxalate	-	+	+	-	+	-
20.	Vitamin C	+	+	+	+	+	+

++ High presence, + Presence and - Absence

Table 4. Qualitative Analysis of Primary and Secondary Metabolites Present in *R. arboreum* Flower Extracts

S.No	Test	Petroleum Ether	Chloroform	Acetone	Ethanol	Methanol	Aqueous
1.	Alkaloids	-	-	+	+	+	+
2.	Flavonoids	-	-	-	+	++	-
3.	Phytosterols	+	+	+	++	++	+
4.	Phenols	+	-	+	++	++	-
5.	Tannins	+	-	+	++	++	-
6.	Diterpenes	-	-	++	++	++	+
7.	Protein	-	-	-	++	++	+
8.	Amino acids	+	-	+	+	+	-
9.	Carbohydrates	-	-	-	+	++	+
10.	Saponins	-	-	-	-	-	++
11.	Quinones	-	+	+	++	++	-
12.	Coumarins	+	-	+	-	+	-
13.	Acidic compounds	+	+	+	-	+	-
14.	Catechin	+	-	++	+	++	-
15.	Volatile oils	+	-	-	-	+	-
16.	Resin	+	-	+	+	+	+
17.	Starch	+	-	-	+	+	±
18.	Carotenoids	-	-	+	-	+	±
19.	Oxalate	+	-	-	-	+	-
20.	Vitamin C	+	-	+	+	+	±

++ High presence, + Presence and - Absence

4.2. Quantitative Estimation of Secondary Metabolites in *R. arboreum*

The quantitative phytochemical analysis of alkaloids, tannins, phenols and flavonoids in *R. arboreum* leaf and flower extracts using methanol, ethanol and acetone as solvents. Methanol leaf extracts of *R. arboreum* had the highest content of 117.1 RE/g TFC followed by 75.95 AE/g TAC, 50.43 TAE/g TTNC and 40.5 mg GAE/g TPC. *R. arboreum* flower methanol extracts of 80.01 TAE/g TTNC had the second highest compound after the highest 139.6 RE/g TFC while the 32.31 AE/g TAC and 47.16 mg GAE/g TPC had moderate levels (Figure. 7 & 8). Whereas *R. arboreum* ethanol and acetone extracts of leaf and flower had lower contents of phytochemicals when compared to methanol extracts.

Antioxidant potential of *R. arboreum* is particularly important because of high TFC as a decisive factor that can counteract oxidative stress and play a role in anti-inflammatory and anticancer activities. Alkaloids have been identified by many studies for their various biological activities, whereas tannins and phenols of the plant together play a role in the antioxidant activity of the plant. The analysis establishes that the use of methanol solvent provides better solubility outcomes at higher concentrations than ethanol or acetone, for methanol possessing higher dissolving activity than other polar solvents (Madhvi *et al.*, 2020).

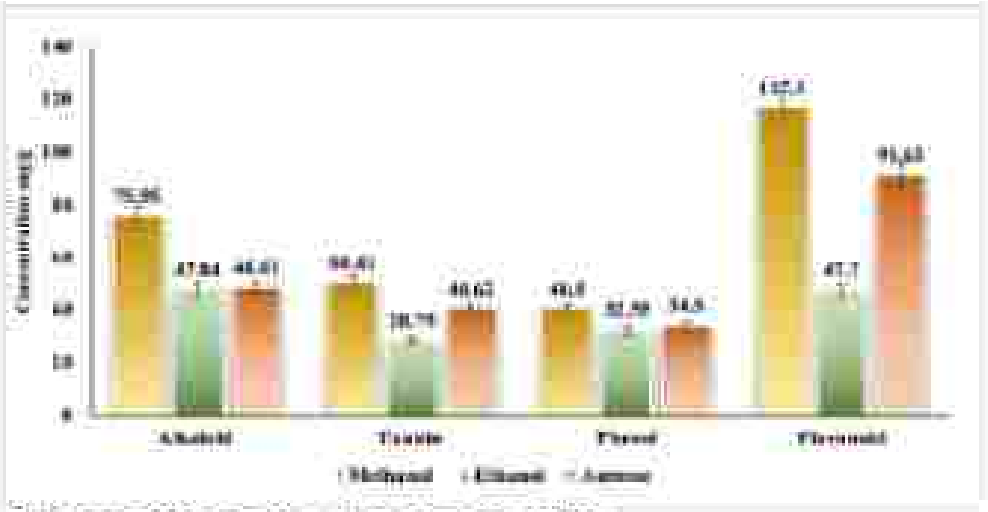

Data expressed as mean ± SEM based on triplicate

Figure 7. Quantitative Estimation of Secondary Metabolites from *R. arboreum* Leaf Extracts

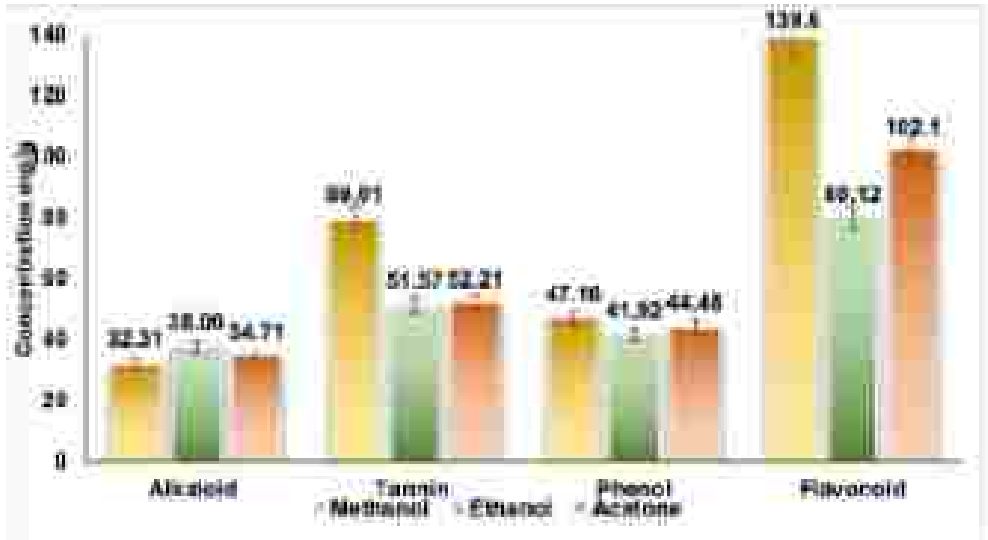

Data expressed as mean ± SEM based on triplicate

Figure 8. Quantitative Analysis of Secondary Metabolites from *R. arboreum* Flower Extracts

In a study conducted by Barola *et al.*, (2022), the highest tannin content (2.98 TAE/g) was reported in 30 g of fresh *R. arboreum* flowers. In contrast, the present study found significant variability in tannin content between leaves and flowers of *R. arboreum*. Leaves exhibited lower tannin content of 28.75±0.02 TAE/g, while flowers showed 51.57±0.03 TAE/g in ethanol extracts. These results highlight the distinct tannin accumulation patterns in different plant parts and underscore the influence of different solvent extraction on tannin quantification.

Rawat *et al.*, (2018) reported significant increase in the total phenolic content (1327.5±0.009 mg GAE/g) in methanolic extracts of *R. arboreum* comparable to other solvents. The present study also showed the highest TFC in RFM (139.6 RE/g) and RLM (117.1 RE/g) and TPC value, the highest value was shown in RFM (47.16 mg GAE/g) and then RLM (40.5 mg GAE/g). There is a combination of high antioxidant capacity in the *R. arboreum* as evidenced by high TFC and TPC values obtained in RFM and RLM. However, this study had lower TPC values than those of Rawat *et al.* this is because of differences in extraction methods. While their study used Soxhlet extraction which uses continuous solvent reflux in increased temperature. In the present study a cold maceration process followed by filtration and rotary evaporation was utilized, this avoids degradation of bioactive compounds due to heat, preserving the composition and giving a more natural representation of their phytochemical composition (Kumar *et al.*, 2023).

Shootha *et al.*, (2022) reported that among the three endemic *Rhododendron* species, *R. maddenii* contained the highest flavonoid content (90.05 QE/g) in methanolic extract, when compared to other solvents followed by *R. ciliatum* with 62.37 QE/g and *R. dalhousiae* with 32.62 QE/g. Similarly the total phenolic content of *R. ciliatum* extract showed the highest values (485.66±13.74 mg GAE/g) followed by *R. dalhousiae* (208.45±9.66 mg GAE/g) and *R. maddenii* (149.56±12.56 mg GAE/g) in methanol extracts. *Rhododendron* species exhibit high abundance of natural antioxidant compounds, resulting in greater phytocompounds accumulations in the methanol solvent. Similarly, the present study also correlated with the above findings with respect to methanolic extract.

4.3. Fourier Transform- Infrared Spectroscopy (FT-IR)

FT-IR spectroscopic analysis detected distinct functional groups in RLM and RFM extracts based on their bonding positions. The resulting peaks conclusively confirm diverse functional groups in the *R. arboreum* leaf and flower extracts.

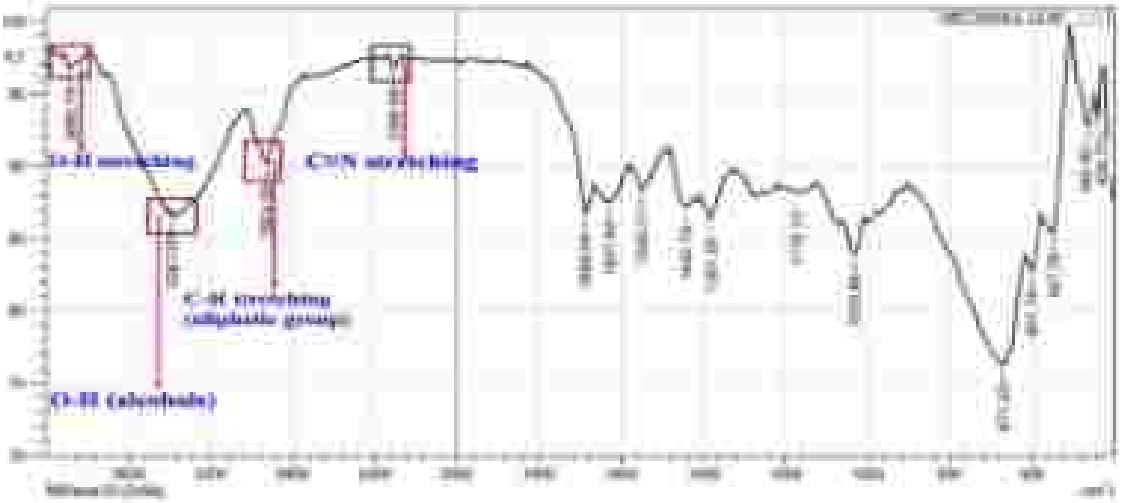

Figure 9. FT-IR of *R. arboreum* Methanol Extract of Leaf

In the present study, FT-IR analysis revealed significant absorbance peaks indicative of various chemical constituents. The RLM showed prominent peaks at wavelengths such as 3680.78 cm^{-1} (O-H stretching, phenols), 3387.00 cm^{-1} (O-H alcohols), 2924.09 cm^{-1} (C-H stretching, aliphatic hydrocarbons), which are consistent with studies conducted on leaves of *Rhododendron arboreum* and *Rhododendron dauricum*, where the strong absorbances at 3379 cm^{-1}, 3400 cm^{-1} and 2930 cm^{-1} were attributed to the stretching vibrations of O-H and C-H, respectively (Mary & Indira, 2017; Hu *et al.*, 2022). 2306.86 cm^{-1} (C≡N stretching) and 1589.64 cm^{-1} (C=O stretching, ketones/aldehydes) (Figure. 9) are consistent with the results of Phuyal *et al.*, 2022.

Similarly, the RFM extract showed distinct peaks at 3718.76 cm^{-1} (O-H stretching, phenols), 3286.70 cm^{-1} (N-H stretching), 2924.09 cm^{-1} (C-H stretching, aliphatic hydrocarbons), 2314.58 cm^{-1} (C≡N stretching) (Figure. 10). FT-IR spectra similar to the spectra reported by Kim *et al.*, 2013, peak at 2922 cm^{-1} were assigned to the C-H stretching, which confirms the probability

of the presence of phenolic compounds. The present findings validates the previous study reported by Ahir *et al.*, (2024) in *R. arboreum*, where the prominent peaks at 3430 cm^{-1} (O-H stretching vibrations) were found in the petal extracts. Hence, the proposed study confirms the constant presence of important functional groups in the extracts of *R. arboreum*.

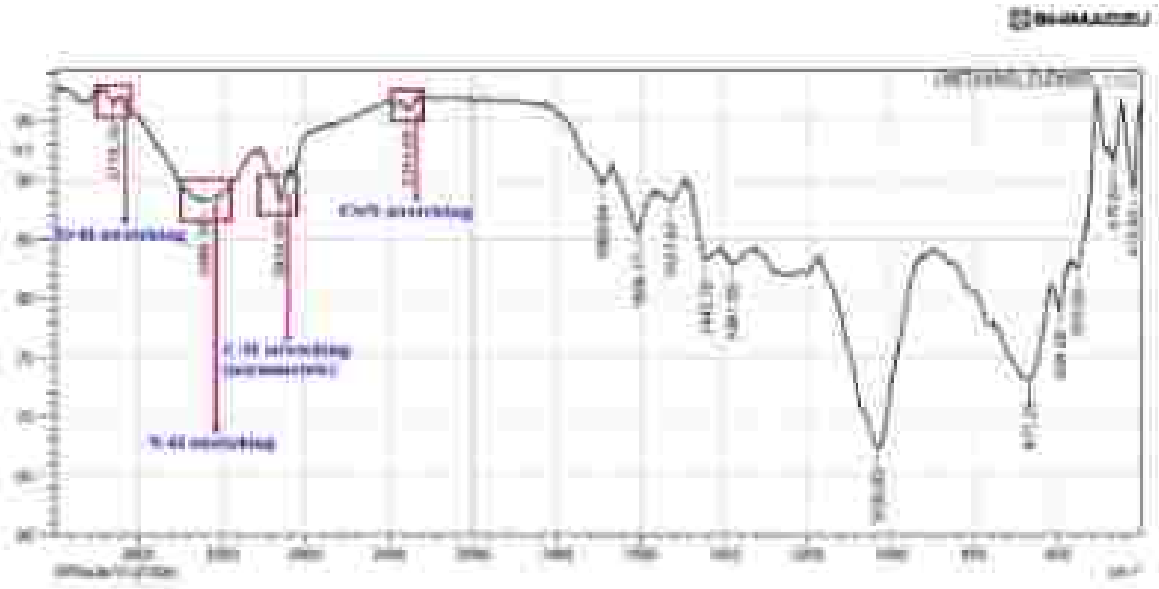

Figure 10. FT-IR of *R. arboreum* Methanol Extract of Flower

4.4. Nuclear Magnetic Resonance (NMR)

NMR is regarded as a non-destructive analytical tool particularly in analysing biomolecular structures. The NMR toolkit encompasses qualitative methods for measuring chemical shift (δ), spin-spin and dipolar couplings (J, providing connectivity) through-space interactions (NOE, also confirming connectivity) and relaxation parameters (T1/T2).

Sixteen metabolites from RLM extracts were detected by ^1H NMR spectroscopy, as shown in Figure 11. The extracts of *R. arboreum* were analysed by NMR spectroscopy to investigate the variations of polar metabolites between the different parts of the plant (RLM and RFM). The biochemical compounds identified in the NMR spectra also showed the presence of different metabolites in RLM and RFM. The detection of the biochemical compounds was further confirmed by comparing the ^1H spectra of the reference compounds with the reference compounds in the Biological Magnetic Resonance Data bank (BMRB) which were also used to characterise

the metabolites (Markley *et al*., 2008). The highest peak corresponds to the aldehyde in the high-field part of the ^{1}H NMR spectra (1.12-5.9 ppm) of the RLM extracts. The signals for the methylene and aliphatic groups were obtained from the lower field region (5-10 ppm).

The proton NMR spectroscopy has been utilized to identify the source of medicinal herbs and herbal products (Kang *et al*., 2008). Rai *et al*., 2023, aimed to identify and isolate the phytoconstituents from the *Rhododendron arboreum* for the immunomodulatory activity and found the presence of ursolic and kaempferol in methanol extracts, which shows the characteristics of aromatic and hydroxyl groups in ^{1}H NMR. It was employed to identify the antitumor screening of alcoholic leaf and flower extracts of *R. arboreum* at *in vitro* level (Sonar *et al*., 2012).

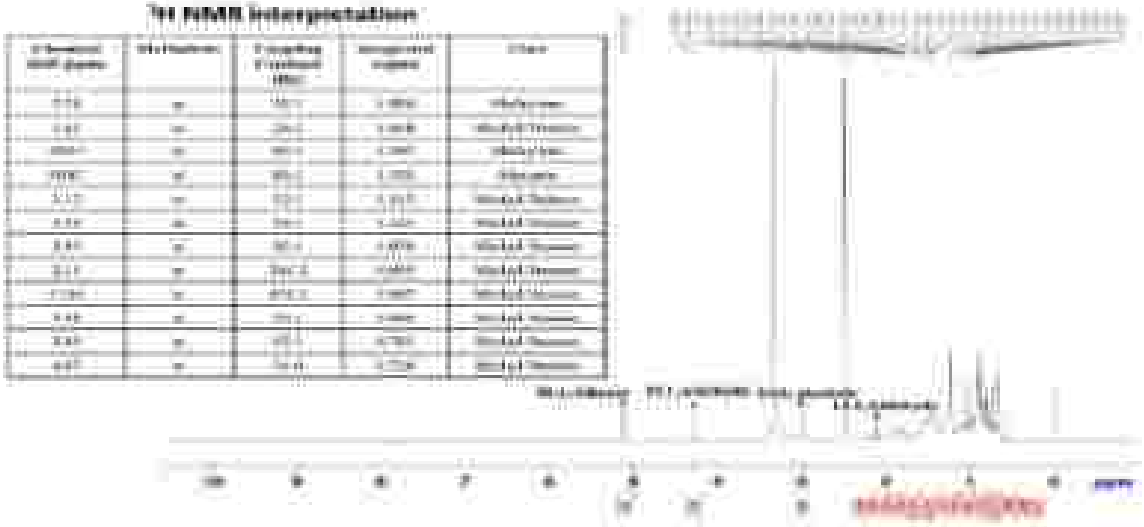

Figure 11. NMR Analysis of *R. arboreum* Methanol Leaf Extract

In the flower extracts of *R. arboreum*, the ^{1}H NMR spectrum highlights diverse chemical factors revealing insights into the chemical groups present in the plant. Multiple peaks across the spectrum correspond to specific chemical shifts, integrated areas and coupling constants, which helps in classifying the protons into aliphatic, aromatic, aldehydic, alcoholic, alkene and alkyl groups (Figure. 12).

^{1}H NMR spectra was used to identify the metabolites by comparing the chemical shift and coupling constant values with typical NMR metabolite peaks from the BMRB data bank. In the high-field region of the ^{1}H NMR spectra

(0.7-2.1 ppm) of RFM extracts, the most abundant peak corresponds to aromatic and aldehyde. In the down-field region (2.1-6.5 ppm) signals were assigned to aldehyde and alkene group-containing compounds (Figure. 12).

The alkene region is represented by a prominent peak at 216.2 Hz consistent with the characteristic deshielding caused by double-bond conjugation. Aromatic protons are identified at 64.0 Hz, where the coupling constants and integration align with the presence of an aromatic ring structure. The alkyl region, with a significant signal at 60.04 Hz confirms protons in a relatively shielded environment possibly near saturated carbon chains. The spectrum also displayed signals in the highly deshielded regions, such as the aldehyde and aromatic zones which indicated the presence of complex and diverse chemical environments within the molecule (Figure. 12).

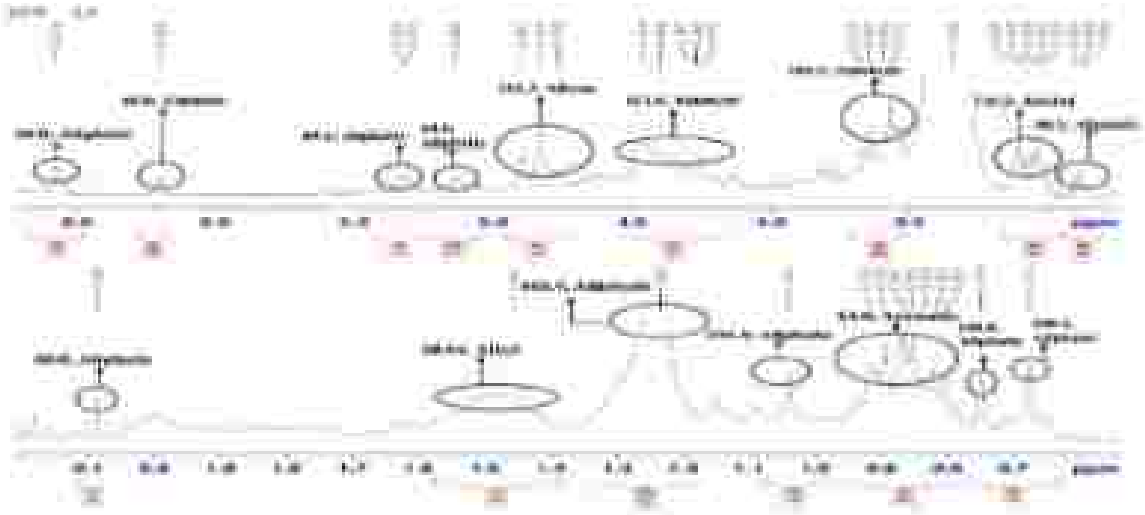

Figure 12. NMR Analysis of *R. arboreum* Methanol Flower Extract

Shagun *et al.*, (2023) revealed that hot aqueous extracts of *R. arboreum* contain quinic acid and chlorogenic acid, aligning with the present study of ^{1}H NMR spectroscopy results characterizing the broader chemical composition of these extracts demonstrating the presence of specific acids providing a foundational understanding of key constituents in *R. arboreum* tissue extracts. Lingwan *et al.*, (2020) also employed ^{1}H NMR spectroscopy for the petals of *R. arboreum*, where they identified various compounds such as quinic acid, coumaric acid, epicatechin, quercetin and kaempferol substances based on their specific chemical shifts and quantities. The analysis included

the correction of spectra for the phase and baseline distortion to ensure its accuracy.

4.5. Gas Chromatography-Mass Spectrometry (GC-MS)

The GC-MS spectrum of the *R. arboreum* leaf extract revealed the presence of several bioactive compounds identified based on their retention time. In the GC-MS chromatogram, several distinct peaks were identified which were assigned to specific compounds using the NIST library.

Overall 20 compounds were discovered in the RLM (Figure. 13) including glycerin; silane; p-Mentha-1(7),2-dien-8-ol; 2,4-dithiapentane; L-alpha-terpineol; carvenone; 2,3-diketo-6-methoxybenzo[b]pyran; phenol; propionic acid; undecane; acetic acid; 2,4-di-tert-butylphenol; 2(4H)-benzofuranone; 1-hexadecanol; cyclohexane; neophytadiene; phytol; eicosanoic acid; hexadecanoic acid and vitamin E. Out of the 20 identified compounds, only 7 were further selected for detailed analysis based on their relevance to the objectives of the present study. These compounds were chosen due to their significant contributions to the observed antioxidant, antimicrobial, anticancer and anti-inflammatory activities which demonstrated critical bioactive properties suitable to the focus of the study.

Hexadecanoic acid, also known as palmitic acid known for its antioxidant properties exhibits increased free radical scavenging activity highlighting its significance in a biological systems (Kim *et al.*, 2006) was observed at retention times of 25.32 and 31.33 indicating its role in lipid metabolism and its known antioxidant and antimicrobial properties. Hosseini *et al.*, (2022) also reported palmitic acid for its crucial role in lipid metabolism and its diverse biological activities. The synthesis of cellular phospholipids along with triglycerides uses palmitic acid as the precursor to create structures required for cell function. The strong antioxidant functions of palmitic acid protect against oxidative stress through lipid and protein oxidation protection mechanisms.

At a retention time of 22.725, 3-buten-2-one an unsaturated ketone was detected which may act as a precursor in biosynthetic pathways. Neophytadiene, a diterpene hydrocarbon with anti-inflammatory and antimicrobial potential was identified at the retention time of 24.382. Willie

et al. (2020) also reported that neophytadiene exhibits diverse biological activities including anti-inflammatory, antimicrobial, analgesic and antioxidant properties in a study conducted for three species of Apocynaceae (*Gongronema latifolium*, *Vincetoxicum rossicum* and *Marsdenia edulis*). These attributes make it a valuable compound which aligns with the present study.

Phytol, a diterpene alcohol derived from chlorophyll degradation and renowned for its antioxidant, anticancer and antimicrobial activities (Alencar *et al.*, 2018) was observed at 27.52 min. Additionally, 2-methylhexacosane, a long-chain hydrocarbon with potential roles in membrane stabilization and biofilm formation was detected at 32.81 min. Vitamin E, a well-known antioxidant that protects cells from oxidative stress and free radical damage appeared at 37.39 min. (Figure. 13). Collectively, all the above compounds highlight the extracts richness in fatty acids, diterpenes, hydrocarbons and vitamins indicating significant antioxidant, antimicrobial, anticancer and anti-inflammatory properties of *R. arboreum* extracts.

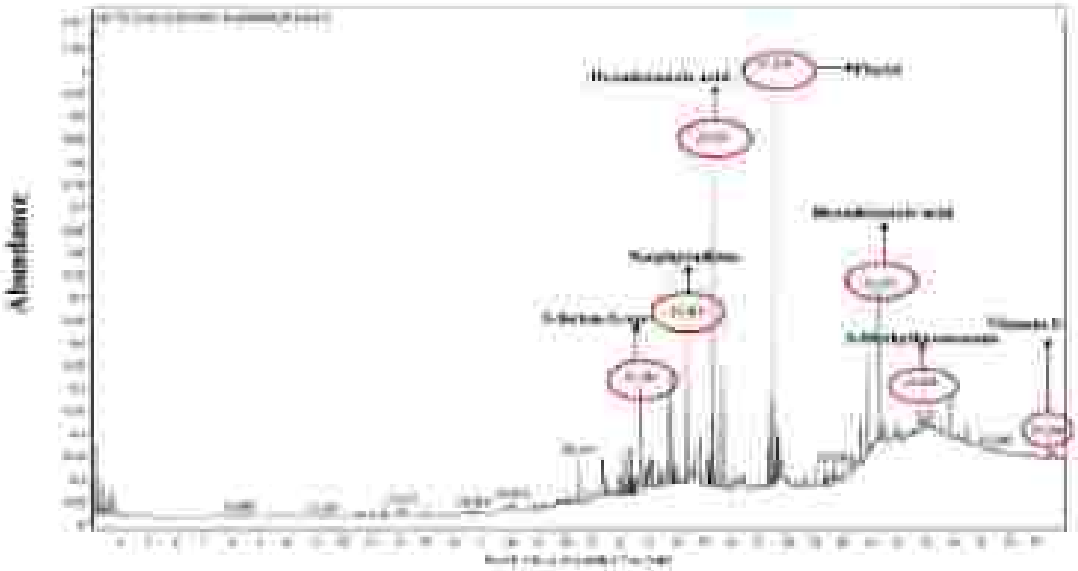

Figure 13. GC-MS Chromatograms of *R. arboreum* Leaf Extract

Similarly, in RFM, a total of 26 compounds (Figure. 14) were detected which includes: Methylenecyclopropanecarboxylic acid; 4-Cyclopentene-1,3-dione; Methyl thiolacetate; 2,4-Dihydroxy-2,5-dimethyl-3(2H)-furan-3-one; 2H-Pyran-2,6(3H)-dione; 2-Cyclopenten-1-one, 2-hydroxy-3-methyl; Furaneol; 3-Acetoxy-3-hydroxypropionic acid; 4H-Pyran-4-one, 2,3-dihydro-3,5- dihydroxy-6-methyl; Benzofuran, 2,3-dihydro; 5-Hydroxymethylfurfural;

Glycerin; beta-Methyl xyloside; 1,2,3-Benzenetriol; 3-Furanacetic acid, 4-hexyl-2,5-dihydro-2,5-dioxo; Ethanol, 2,2'-oxybis-, diacetate; Phthalic acid, 2-isopropylphenyl methyl ester; beta-l-Arabinopyranoside, methyl; n-Hexadecanoic acid; 9,12-Octadecadienoic acid (Z,Z)-, methyl ester; 4-Imidazolidinecarboxylic acid, 4-hydroxy-2,5-dioxo; Hexadecanoic acid, 10-hydroxy-, methyl ester; Hexadecanoic acid, 2-hydroxy-1- (hydroxymethyl)ethyl ester; gamma.-Sitosterol; 5H-Oxazolo[3,2-a]pyridine-8- carbonitrile, 6-ethyl-2,3-dihydro-2,7-dimethyl-5-oxo- and α-amyrin. Out of the 26 compounds identified from RFM, only 9 were further prioritized based on their relevance to the objective of the present study.

α-amyrin at 34.42 min. is a triterpene known for its antioxidant, anti-inflammatory and antimicrobial properties. Baburaj *et al.*, (2022) also reported the biological activities of α-amyrin which aligns with the present study emphasizing its pronounced anti-inflammatory properties. The study reported that α-amyrin exhibited dose-dependent inhibition in various *in vitro* anti-inflammatory assays such as albumin denaturation, anti-proteinase and anti-lipoxygenase activities. Gamma-sitosterol at 32.78 min. is a plant sterol with demonstrated antioxidant and lipid-regulating effects (Surya *et al.*, 2023).

Octadecadienoic acid at 27.31 min. commonly known as linoleic acid exhibits antioxidant and anti-inflammatory properties. β-L-arabinopyranoside at 22.978 min. is a sugar derivative that contributes to the bioactive profile of the extract. Benzofuran at 13.58 min. is known for its antioxidant, anticancer and antimicrobial activities. Farhat *et al.*, (2022) reported that benzofuran derivatives demonstrate significant anticancer activity against various human cancer cell lines. The study found the importance of structure-activity relationships (SAR) in determining their efficacy, reporting that specific substitutions on the benzofuran scaffold can modulate cytotoxicity. Furthermore, benzofuran derivatives are emphasized as promising candidates for novel therapeutic agents due to their selectivity against cancer cells and their potential to inhibit tumour progression with minimal adverse effects (Farhat *et al.*, 2022). 2-Propenoic acid at 11.76 min. and 1,2-cyclopentanedione at 5.92 min. are compounds with reported antioxidant and antimicrobial effects (Guglu, 2024). Methylenecyclopropane carboxylic

acid at 4.893 min. and 1,4-dioxane-2,6-dione at 3.673 min. further enhance the extract's bioactive properties, particularly in terms of antimicrobial and antioxidant potential (Wei *et al.*, 2023).

Figure 14. GC-MS Chromatograms of *R. arboreum* Flower Extract

4.6. Free Radical Scavenging Activity of *R. arboreum* Leaves and Flowers Extract

4.6.1. DPPH Radical Scavenging Assay

The antioxidant potential of RLM and RFM was evaluated using the DPPH scavenging assay. Both extracts exhibited substantial antioxidant activity, demonstrating effectiveness comparable to the standard (ascorbic acid). The assay relies on the ability of DPPH, a stable free radical to change colour (from purple to yellow) upon reduction by antioxidants.

The methanol extracts from both leaves and flowers of *R. arboreum* showed significant inhibition of DPPH activity. Specifically, the IC_{50} values for the methanol extracts of RLM and RFM were determined to be 56.8±1.91 µg/mL and 67.3±2.95 µg/mL respectively, indicating their potent antioxidant capabilities (Figure. 15). Similarly, Bhatt *et al.*, (2022) reported the increased antioxidant potential of the flower extracts. The percentage of inhibition was calculated using the absorbance values of the DPPH solution before and after the addition of the sample. The results indicated that the extracts exhibited significant antioxidant activity, with IC_{50} values

(concentration required to inhibit 50% of the DPPH radicals) of 102.06 and 96.92 µg/mL for different extracts, reporting a strong capability of the samples to neutralize free radicals.

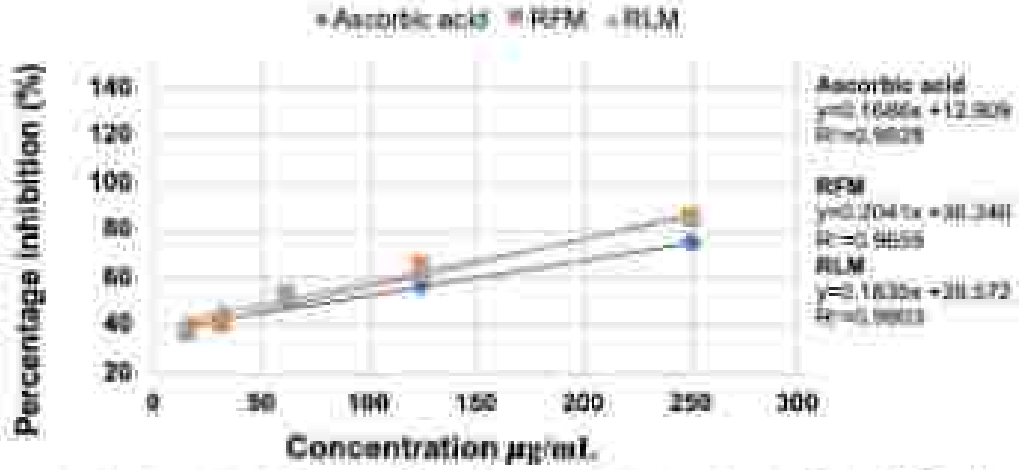

(Experiments done in triplicates and IC_{50} values were determined using Microsoft Excel by linear regression plotted from concentration vs. % inhibition)

Figure 15. DPPH Radical Scavenging Activity of *R. arboreum* Leaf and Flower Extracts

Winitchai *et al.*, 2021 reported higher antioxidant activity in *R. arboreum* dried leaf (IC_{50} = 24.65±1.47 µg/mL) compared to dry flower (42.34±1.13 µg/mL) and fresh flower (48.15±1.65 µg/mL) extracts. The present evaluation also emphasizes the strong antioxidant potential of RLM when compared to RFM. Jha *et al.*, (2024) reported that the different extracts of *R. arboreum* (aqueous extract - LGP, ethanolic extract - LGE and acetone extract - LGA) exhibited significant DPPH radical scavenging activity, indicating their antioxidants potential.

4.6.2. ABTS(2,2'-azino-bis(3-ethylbenzothiazoline-6-sulfonic acid)) Radicals

The ABTS cation assay was employed to evaluate the scavenging activity of RLM and RFM. The assessment was performed using a concentration ranging from 50-300 µg/mL. The methanol extract of leaves exhibited an IC_{50} value of 60.7±2.13 µg/mL, while the flower extract showed an IC_{50} value of 65.9±1.97 µg/mL. This indicates that both extracts possess significant antioxidant potential with the RLM extract demonstrating slightly stronger scavenging activity against ABTS radicals compared to the RFM

extract (Figure: 16). The ABTS assay measures the ability of antioxidants to quench the ABTS radical cation, reflected in a decreased absorbance at 734 nm.

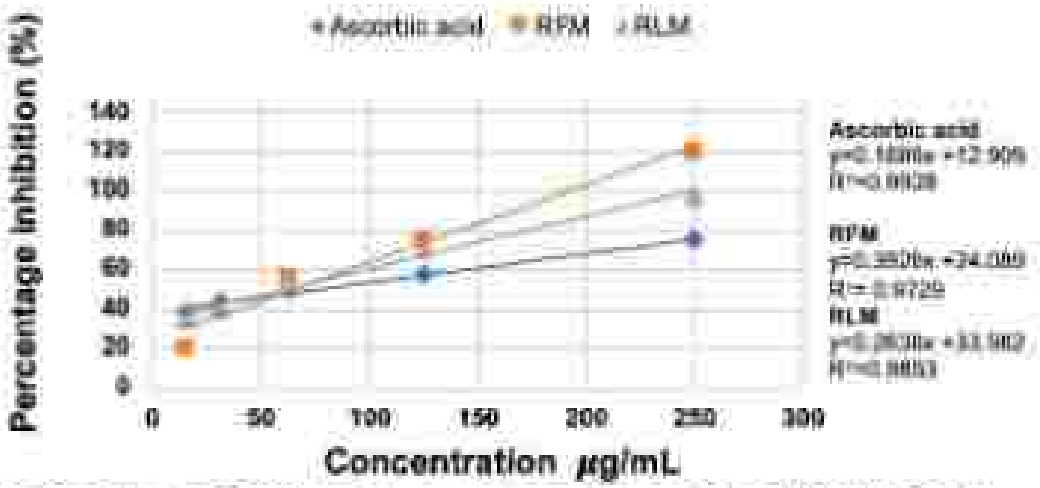

(Experiments done in triplicates and IC_{50} values were determined using Microsoft Excel by linear regression plotted from concentration vs. % inhibition)

Figure 16. ABTS Radical Scavenging Activity of *R. arboreum* Leaf and Flower Extracts

These suggest variability in antioxidant activity depending on the plant parts and their extraction methods. Bhatt *et al.*, (2022) conducted an ABTS radical scavenging assay to evaluate the antioxidant potential of *R. arboreum* flower extracts. In their study, the ABTS radical cation absorbance was measured before and after the addition of plant samples. The results indicated that the extracts exhibited significant antioxidant activity. Similarly, Sharma *et al.*, (2021) reported that the methanolic extract of *R. arboreum* flowers had the highest ABTS radical activity with an IC_{50} of 11.49±1.25 µg/mL indicating potent antioxidant capability. The observed variation in the IC_{50} values for all the above studies on the *R. arboreum* flower extracts attributes to several factors such as geographical location, environmental conditions and the time of year or developmental stage at which plant material was collected significantly impact the chemical composition of the extracts (Palit & Mandal, 2021; Sukmawaty *et al.*, 2024). The above studies observed antioxidant activity and their bioactive constituents, play a crucial role in scavenging free radicals.

4.6.3. H_2O_2 (Hydrogen Peroxide) Scavenging Activity

The IC50 values for the RLM was found to be 53.5±1.36 µg/mL, whereas the RPM showed the results as 57.6±2.72 µg/mL. These results indicated that

both extracts possess significant antioxidant potential against H_2O_2-induced oxidative stress. RLM exhibiting slightly higher scavenging activity compared to the RFM (Figure. 17). The H_2O_2 scavenging assay measures the ability of antioxidants to neutralize H_2O_2, thereby reducing oxidative damage. The ability of methanol extracts from both the leaves and flowers of *R. arboreum* to scavenge hydrogen peroxide as indicated by their respective IC_{50} values was significantly different ($p < 0.05$) when compared to the IC_{50} values obtained from ascorbic acid (standard).

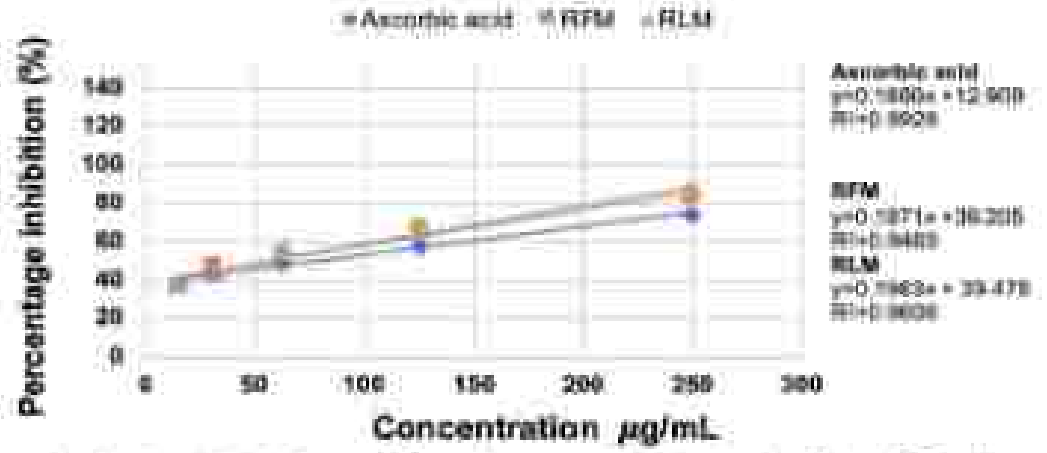

(Experiments done in triplicates and IC_{50} values were determined using Microsoft Excel by linear regression plotted from concentration vs. % inhibition)

Figure 17. Hydrogen Peroxide Radical Scavenging Activity of *R. arboreum* Leaf and Flower Extracts

Wan *et al.*, 2022, evaluated the antioxidant effects of polysaccharides from *Sargassum fusiforme*. H_2O_2 exposure increased reactive oxygen species levels (ROS). The protective effect suggested the potential against the oxidative stress, with lower molecular weight fraction proving more effective in penetrating cell membranes to exert their benefits. The H_2O_2 scavenging assay assesses the ability of antioxidants to neutralize H_2O_2, thereby protecting cells from oxidative damage (Zhang *et al.*, 2006).

4.6.4. Lipid Peroxidation Inhibition Assay (LPO)

RLM and RFM were determined to be 56.6±2.50 µg/mL and 80.4±1.21 µg/mL respectively. Both RLM and RFM extracts significantly demonstrated higher LPO activity compared to ascorbic acid alone ($p < 0.01$) (Figure. 18). These results highlight the superior antioxidant efficacy of *R. arboreum* extracts, reporting the potential therapeutic utility in preventing oxidative

damage associated with lipid peroxidation.

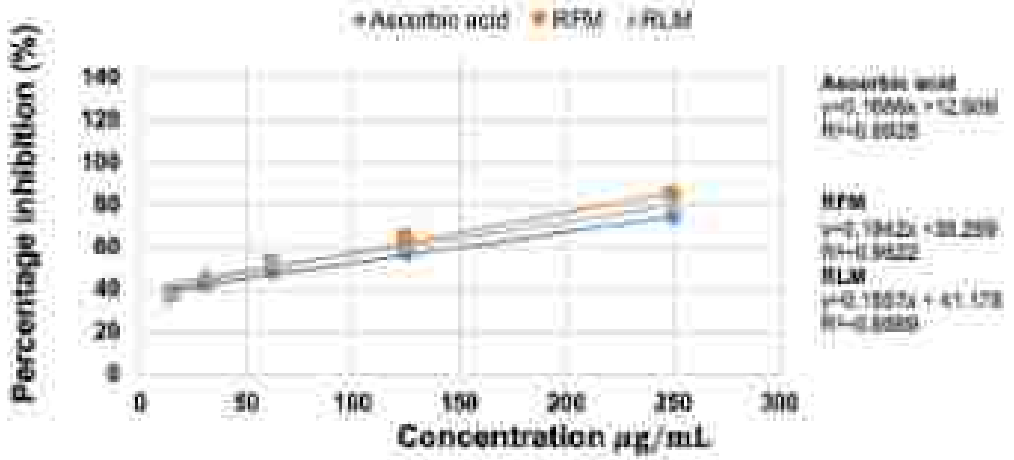

(Experiments done in triplicates and IC_{50} values were determined using Microsoft Excel by linear regression plotted from concentration vs. % inhibition)

Figure 18. Lipid Peroxidation Assay *R. arboreum* Leaf and Flower Extracts

According to Acharya *et al.*, (2011), the potent inhibition of lipid peroxidation by the ethanolic extract of *R. arboreum* with an IC_{50} value of 45.6 µg/mL. In accordance with their findings, the present study investigated RLM and RFM for LPO. The result showed the IC_{50} values of 56.6±2.50 µg/mL for the RLM and 60.4±1.21 µg/mL for the RFM. This aligns with the findings of previous study, revealing that *R. arboreum* extracts has the potential in inhibiting lipid peroxidation regardless of solvent used. Similarly, Gautam *et al.*, 2020, reported that the antioxidant activity of the methanol extract of *R. arboreum* leaves with an IC_{50} value of 103.6 mg/mL in LPO assay. This reports that the antioxidant potential of *R. arboreum* extracts is dose-dependent and is attributed to the presence of bioactive phytochemicals that effectively scavenge or inhibit free radicals production.

Paul *et al.*, (2023) reported on lipid peroxidation assay, using the measurement of malondialdehyde (MDA) content which is an end product of lipid peroxidation. The study found that the levels of MDA were significantly reduced in treated cultures compared to control and untreated samples. Specifically, the treated cultures exhibited a significant decrease of 50.43% in MDA content when treated with 1% *R. arboreum* flower methanol extract in a neurodegeneration model induced by 120 µM H_2O_2. This reduction indicates that the bioactive compounds in *R. arboreum* flower methanol extract have the ability to mitigate oxidative stress, thereby lowering the production of MDA

and indicating a protective effect against oxidative damage in the brain.

4.6.5. Ferric Reducing Antioxidant Power (FRAP)

The results of the Ferric Reducing Antioxidant Power (FRAP) assay for RFM and RLM extracts are depicted in the graph (Figure. 19), which demonstrate a clear trend in antioxidant activity across varying concentrations (0 to 250 mM). Both RFM and RLM exhibited increasing FRAP values with higher concentrations, indicative of enhanced reducing power. Significantly, the RFM consistently showed greater FRAP values than RLM at all tested concentrations which reports that the flower extracts possess more potent antioxidant capacity than the leaf extracts. This emphasizes the potential of *R. arboreum* flowers as a richer source of bioactive compounds that contribute to antioxidant activity.

Additionally, both extracts displayed an elevated effect in FRAP values at concentrations up-to 200-250 mM, indicating a saturation point beyond which no significant difference was observed. These results suggest that *R. arboreum* possesses significant antioxidant properties particularly in RFM, which may be beneficial for targeted oxidative stress-related conditions.

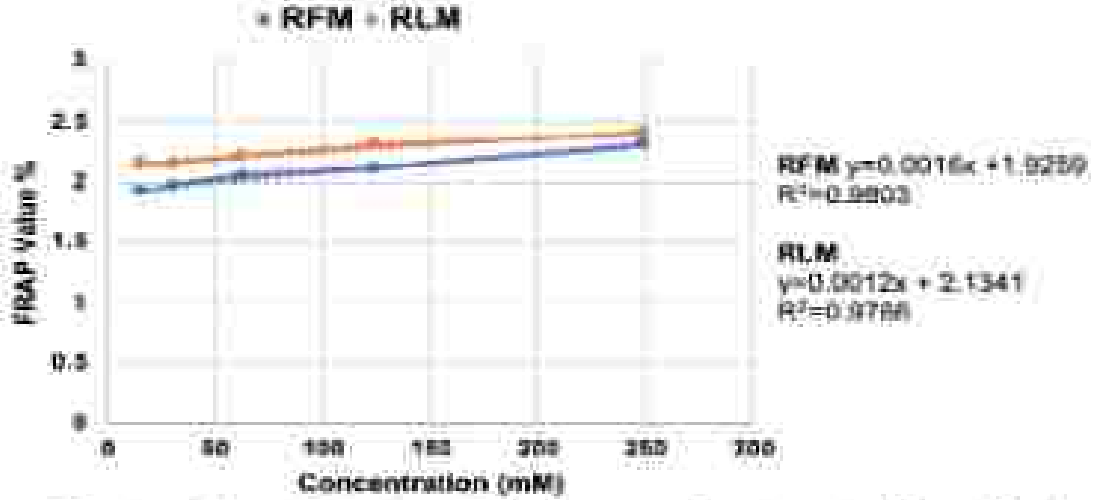

(Experiments done in triplicates and IC_{50} values were determined using Microsoft Excel by linear regression plotted from concentration vs. % inhibition)

Figure 19. FRAP Radical Scavenging Activity of *R. arboreum* Leaf and Flower Extracts

In alignment with the findings of Kashyap *et al.*, (2017) a high FRAP value of 140.6±2.76 mM TE/g for *R. arboreum* flower extract, in the present findings also showed a significant antioxidant potential of RFM. While

the specific FRAP values in present study indicated a comparable trend, resulting in further emphasizing of the antioxidant activity in both RFM and RLM extracts that correlates with the concentration of polyphenolic compounds present in these plant parts as a source of the potent antioxidants.

Similarly, Sharma et al., (2021) evaluated the antioxidant activity of various parts of *R. arboreum* using FRAP assay, observed an increasing activity with increase in concentration of solvent extracts from various parts of *R. arboreum*. Among all extracts, the methanolic extract of the flower exhibited the highest FRAP activity with an IC_{50} value of 22.78±0.39 µM followed by the aqueous extract of the flower with an IC_{50} of 33.78±1.39 µM. The methanolic extract of the leaf showed lower FRAP activity (333.52± 30.14 µM) while the water extract of the leaf had the least activity among the extracts tested.

These studies report that the flower extracts, particularly those obtained using methanol and aqueous, possess significant antioxidant potential likely due to their higher total phenolic and flavonoid content. Hence, the present results corroborate with previous study by confirming the antioxidant potential of *R. arboreum* extracts. While they reported methanolic flower extract as a potent antioxidant with an IC_{50} of 22.76 µM. The present study showed IC_{50} values of 56 mM for RLM and 63.4 mM for RFM. Therefore both studies highlight the significance of *R. arboreum* as a source of increased antioxidants potential.

4.7. Toxicity Study- Brine Shrimp Lethality Assay

The results on the lethality of RFM and RLM extract on brine shrimps was recorded and the data were depicted in Table 5. The both samples (RFM, RLM) was comparatively less toxic than $K_2Cr_2O_7$ (potassium dichromate) which showed maximum lethality of shrimps at higher concentration. The shrimps in the samples (RFM, RLM) were found to be very less toxic in lower concentration (100-500 µg/mL) as well as in higher concentration (1500 µg/mL). Even after 24 hours, only 1 to 4 shrimps were found to be mortal at highest concentration.

Table 5. Brine Shrimp Lethality Assay

S. No	Sample Code	Concentration (µg/mL)	Mortality of Brine shrimp (No. of shrimps dead) (Hours)					
			1	2	4	6	24	% Mortality (at 24 h)
1.	RFM	100	0	0	0	1	1	3
		250	0	1	1	1	1	3
		500	0	0	2	2	2	7
		1000	0	2	2	2	3	10
		1500	0	0	2	3	3	10
2.	RLM	100	0	0	0	0	0	0
		250	0	0	0	2	2	7
		500	0	0	1	2	2	7
		1000	0	0	2	4	4	13
		1500	0	1	1	2	4	13
3.	Control($K_2Cr_2O_7$)	1 (mg/mL)	10	-	-	-	-	100
4.	Blank	Saline water	0	0	0	0	0	0

Using brine shrimp lethality bioassay RFM and RLM were investigated to predict the toxicity of the chemicals on normal shrimps. The study revealed that both RFM and RLM exhibited lower toxicity when exposed to brine shrimps. The comparison of RFM and RLM concentrations with the mortality rate of brine shrimps, revealed that dose-dependent increase in mortality. This indicates that the substance could be potentially toxic given its LC_{50} is approximately 1000 µg/mL.

The toxicity test results showed that RLM caused the highest mortality rate in the tested shrimps (13%) followed by RFM (10%). Based on the available literature data, there is a significant scarcity of research studies dedicated to evaluate the *in vitro* toxicity of *R. arboreum* by observing the effects on brine shrimp larvae (*Artemia salina*).

Bharathy *et al.*, (2024) tested the cytotoxic effects using brine shrimp lethality test the result revealed that *R. arboreum* exhibited less cytotoxicity at lower concentrations (40 µg/mL) resulting in a 10% mortality rate, while a higher concentration of 80 µg/mL led to a 20% mortality rate. The calculated LC_{50} for the formulation was approximately 30.5 µg/mL, indicating that

the extracts have relatively low toxicity levels.

Judzentiene *et al.*, (2022) examined *in vivo* toxic properties of essential oils (Eos) from inflorescences and leaves of *Helichrysum arenarium* L. wild plants, tested with brine shrimp (*Artemia salina*) larvae, indicating diverse LC_{50} average values ranging from 11.23 to 20.50 µg/mL. Similarly, Marsh rosemary (*Rhododendron tomentosum* H) inflorescence oil (3 FI) demonstrated lower toxicity showing an LC_{50} value of 20.50 µg/mL. According to the National Cancer Institute of the United States of America, crude extracts of plants that could potentially be used as anti-cancer agents should have an LC_{50} less than 20 µg/mL (Isa *et al.*, 2016). The present findings on the lethality test for *R. arboreum* extracts found significant anti-cancer activity with LC_{50} values indicating their potential in cancer research.

The present study monitored the number of deceased shrimps for each sample concentration after 24 hours and the results align with the findings reported in previous studies carried out. In the current study, the lethality test results for RFM and RLM showed LC_{50} values of 18.45 µg/mL and 13.83 µg/mL respectively. The study provides insights into the toxicity levels of RFM and RLM significance.

4.8. Cytotoxicity Assay using AGS (Human Gastric Adenocarcinoma Cell-Line)

4.8.1. Cell Proliferation Assay

Cell viability was assessed using the MTT assay to evaluate the cytotoxic activity of RLM and RFM extracts on AGS cells. The methanol extract of RLM exhibited the highest cytotoxic effect against AGS cell lines with a percentage (%) inhibition ranging from 43.5% at the lowest concentration (125 µg/mL) to 66.2% at the highest concentration (1000 µg/mL) (Figure. 20). Following closely, RFM displayed cytotoxic effects ranging from 46.7% at 125 µg/mL to 59.9% at 1000 µg/mL on AGS cell lines (Figure. 21). The analysis of cytotoxicity for the RFM and RLM revealed significant cytotoxic activity with IC_{50} values of 165.6 µL/mL and 270.7 µl/mL respectively.

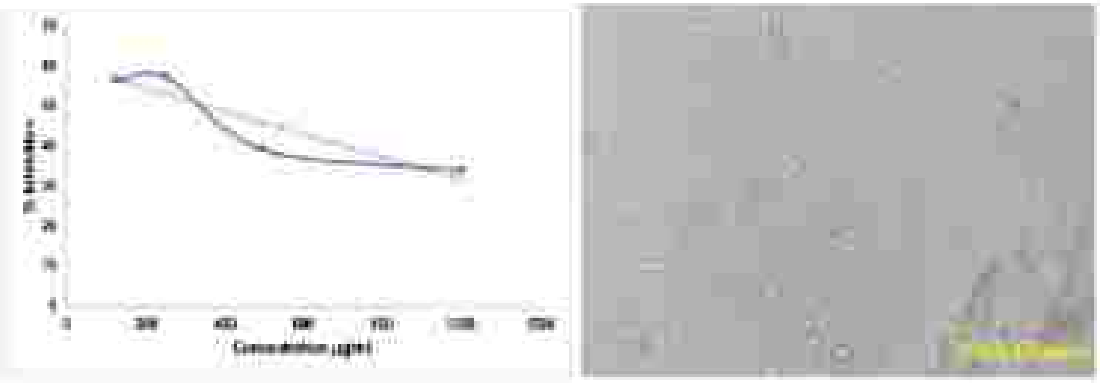

Figure 20. Cytotoxicity of Leaf *R. arboreum* on AGS Cell Line (Results are presented as % cell inhibition and log_{10} concentration using Graph Pad prism software).

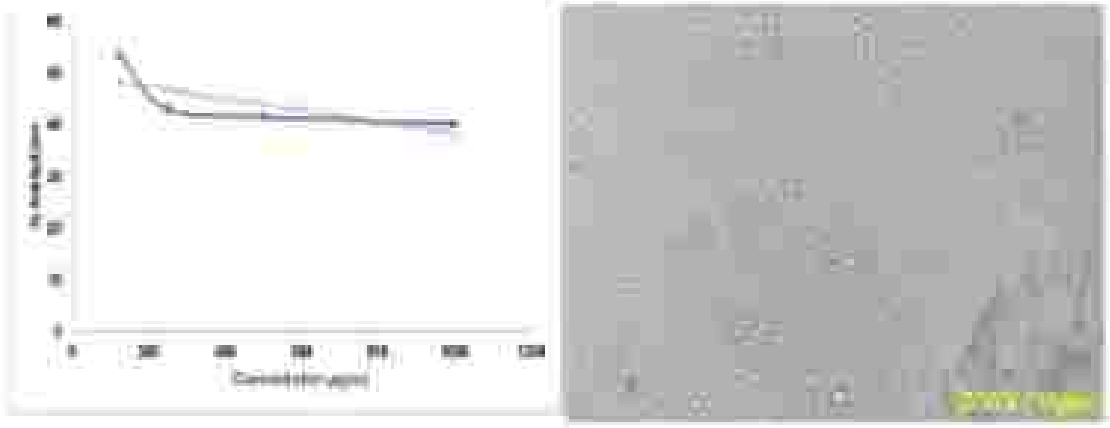

Figure 21. Cytotoxicity of Flower *R. arboreum* on AGS Cell Line (Results are presented as % cell inhibition and log_{10} concentration using Graph Pad prism software).

In investigating the potential anti-cancer effects of RLM and RFM extracts on AGS cells, the present study confirmed that the inhibitory impact on AGS cell proliferation was contingent upon the concentration of samples and the initial cell density. Even at a concentration as high as 1000 µg/mL, the RLM and RFM extract exhibited significant inhibition particularly against densely populated AGS cells. Following 24 and 48 hours of incubation with RLM and RFM extracts respectively, a substantial and significant inhibition of AGS cells was observed. These results suggest that RLM and RFM extracts may contain a diverse array of cytotoxic agents indicating potential applications in the treatment of cancerous cells.

A study conducted by Liu *et al.*, (2021) identified compound a2, a novel derivative of Jiyuan oridonin A (JDA) which exhibited significant anti-cancer

efficacy against gastric cancer cells. They reported that a2 effectively inhibited cell growth with GI_{50} (Growth Inhibition) values ranging from 0.88 to 3.33 mM/L across various gastric cancer cell lines demonstrating its selective action compared to normal gastric epithelial cells. The mechanism of action was elucidated, revealing that a2 induces ferroptosis, a form of programmed cell death characterized by the accumulation of reactive oxygen species (ROS) and primarily through the down-regulation of GPx4.

A study investigated the impact of *Ocimum tenuiflorum* essential oil (OTEO) on the viability of AGS gastric cancer cells using the MTT assay by Boonyanugomol *et al.* (2021). AGS cells were treated with varying concentrations of OTEO. The results indicated a reduction in cell viability with increasing concentrations of OTEO; specifically, at 62.50 µg/mL, 87.4% of the cells remained viable compared to the control group while at 125 µg/mL, viability dropped to 59.83% and at 250 µg/mL, only 37.47% of the cells were viable ($p < 0.05$). Significantly, at a concentration of 500 µg/mL, OTEO completely inhibited AGS cell viability, meaning none of the cells survived. The IC_{50} value was found to be 163.42 µg/mL, at this concentration half of the AGS cells would be expected to be non-viable.

4.9. Detection of Apoptosis using Flow cytometer Analysis

To distinguish between apoptosis in RFM and RLM, treatment cells were harvested and stained with Annexin V-FITC and PI. The combination of Annexin V and PI is widely used to assess the different stages of apoptosis in drug-treated cells (Manogaran *et al.*, 2023). The results showed that apoptosis was higher in the RFM cells compared to RLM (Figure. 22). The cytotoxicity study of plant extracts was also correlated with the present results.

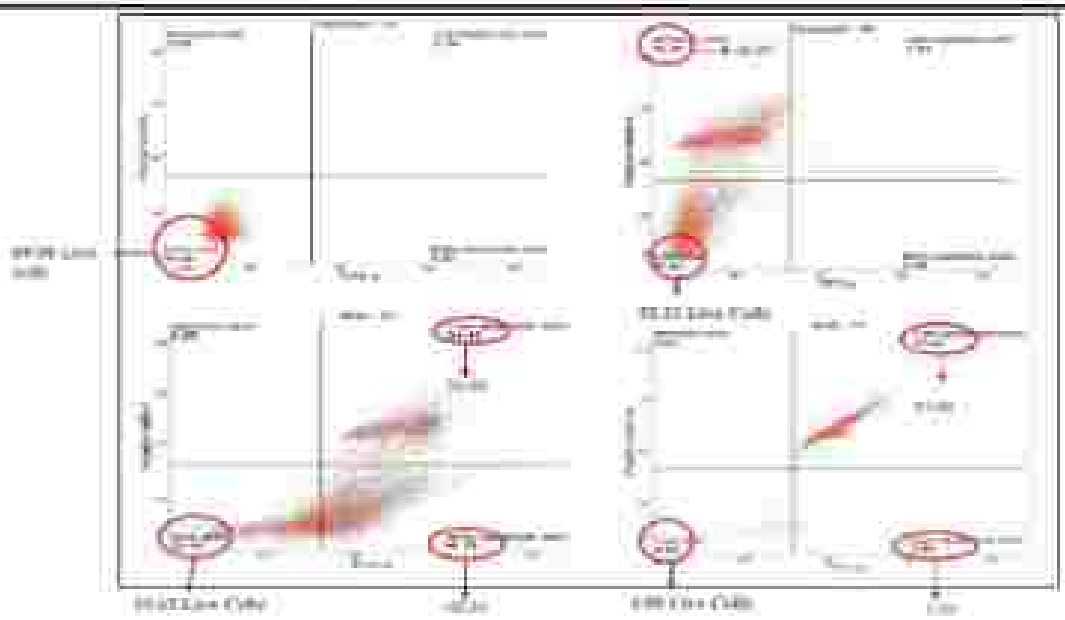

Figure 22. Flow Cytometry Analysis of *R. arboreum* Flower and Leaf Extracts

A study conducted by Boonyanugomol *et al.*, in 2021, the detection of cell death in the study performed using Annexin V-FITC and propidium iodide (PI) staining followed by analysis with a flow cytometer. This method is widely utilized to differentiate between live and necrotic cells. During flow cytometer analysis, cells are stained with both Annexin V-FITC and PI and the flow cytometer measures the fluorescence intensity of each cell. This allows for the identification of different populations: live cells (Annexin V negative, PI negative), early apoptotic cells (Annexin V positive, PI negative) and late apoptotic or necrotic cells (Annexin V positive, PI positive). The present study of *R. arboreum* aligns with above study using Annexin V-FITC and PI staining to differentiate between live and necrosis in AGS cells treated with *Rhododendron* flower and leaf extracts. The studies emphasize the utility of this dual staining method to comprehensively assess cell death mechanisms with the present study results indicating higher apoptosis in RFM compared to RLM cells.

4.9.1. Evaluation of Cell Apoptosis

The present study investigated the apoptotic effect of RFM and RLM on AGS cells in order to understand how RFM and RLM plays an important role in controlling tumor growth. Microscopic observation revealed the distorted nuclei

and shrunken nuclei after the treatment.

A treatment (48 hours) with 1000 µl/mL was slightly toxic to normal cells for both RFM and RLM extracts, aligning with the acceptable toxicity for cancer cells 50% survival. The RLM extract did not harm the cells much, but at a concentration of 1000 µl/mL it significantly slowed down their growth, even though this concentration was most effective against cancer cells, it also affected the survival of normal cells by reducing their viability.

The present finding showed a significant increase in the reduction of cancer cell survival with an increase in treatment concentration. Although this was somewhat similar for normal cells, indicating a potential response between cancer and normal cells.

In Annexin V-FITC/PI, staining was used to quantify apoptotic cell percentage. The results demonstrate a concentration-dependent increase in the rate of apoptosis induced by RFM and RLM extracts in AGS. This signifies the cytotoxic potential of these extracts through the promotion of apoptosis. As reported by Guo *et al.*, 2024, apoptosis is characterized by distinct morphological alterations, including membrane swelling, cellular shrinkage, chromatin condensation and the formation of apoptotic bodies.

4.10. *In vivo* Studies on Docetaxel-Induced Experimental Mice Model

4.10.1. Successful Establishment of the Mice Model

Intervention with chemo-preventive agents can be strategically targeted at various stages of multistage carcinogenesis, namely initiation, promotion or progression (Swetha *et al.*, 2022). Among these stages, the promotion stage appears to be the most feasible and effective for practical application. The study aims to evaluate the potential of *Rhododendron arboreum* DMSO extracts from flowers and leaves (RFD & RLD) in inhibiting gastric cancer in a C57BL/6 mice model.

The animals were acclimatized for one week at room temperature before AGS cells were inoculated on the 7th day. Tumor development in the antrum was detected on the 18th day (Figure. 23). Treatment with the standard drug docetaxel, RFD and RLD extracts started 4 days after tumor detection and

continued for 27 days. During treatment, a high mortality rate was observed in the AGS cell only group. Subsequent analyses included haematological parameters, biochemical analysis, and histological examinations were also done.

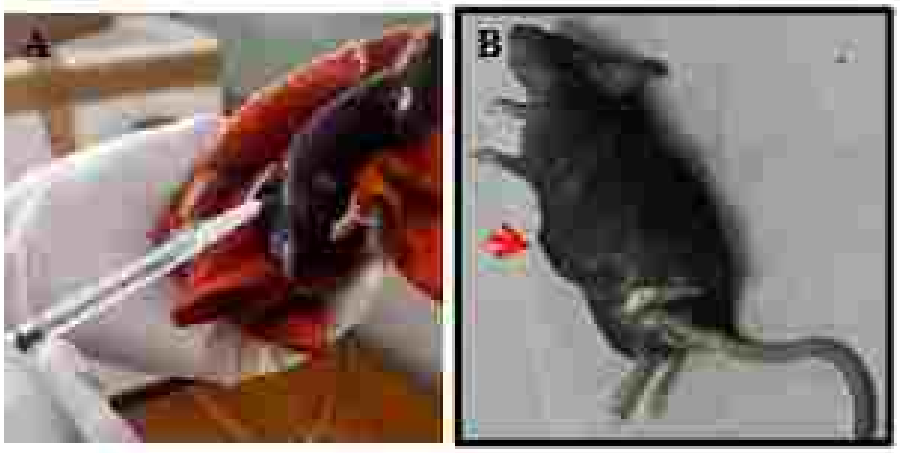

Figure 23. C57BL/6 with Tumor Development. **(A)** Induction of AGS- Gastric Cancer Cell in C57BL/6 Mice Subcutaneously **(B)** Red Arrows Indicate the Subcutaneous Tumour of the Antrum.

4.10.2. Treatment Resisting Body Weight and Tumour Burden

Initial body weights were recorded, with Group I averaging 20.6±1.86 g. Changes in body weight were observed across treatment groups compared to initial measurements. Organ weight data in C57BL/6 mice under different treatments showed varied effects on stomach weight, with further deviations noted in combinations with standard treatment and plant extracts (Table. 6) respectively, at a dosage of 200 mg/kg body weight combined with AGS induction, varying degrees of tumor development were observed (Figure. 27).

Table 6. Body Weight and Organ Weight of C57BL/6 Mice Models

Groups	Group I	Group II	Group III	Group IV	Group V	Group VI	Group VII
Initial Body Weight (g)	20.6±1.86	21.8±0.96	27.1±1.77	25.6±0.70	32.1±3.11	29.1±2.22	30.5±1.96
Final Body Weight (g)	31.1±1.57	19.3±3.21	22.6±5.29	22.6±5.07	19.6±3.9	14.4±5.48	14.5±5.54
Stomach Weight (g)	0.25±0.02	0.21±0.04	0.16±0.03	0.20±0.05	0.10±0.03	0.11±0.04	0.17±0.06

4.11. Estimation of Haematological Parameters

C57BL/6 mice with AGS tumor cells were used to evaluate the anti-hematologic neoplasm effect of RLD and RFD extracts. After treatment, mice were sacrificed. Groups II, VI and VII showed a significant increase in RBCs count compared to Group I. WBCs in group III were a bit elevated; this could be because of the body responding to the inflammation or an infection, especially when the treatment involves chemotherapy drugs (Sankar & villa, 2021). Stress in the body leading to a temporary increase in WBCs production as the body attempts to defend itself.

The content of haemoglobin also appears to be different across the groups. While the control group (group I) consistently maintained normal levels at 16.4±0.36 g/dL, the untreated group presented a slight decrease (13.4±0.34 g/dL) indicating tumor-related anaemia. It was found that the standard drug (group III) increased haemoglobin levels modestly enough to 14.7±0.55 g/dL, although no sufficient progress in control restoration was achieved (Table 7). The RFD extract at low dose (13.9±1.57 g/dL) was able to reveal some recovery in relation to the untreated group (I) but the high dose produced a more pronounced decline (12.7±0.69 g/dL, $p < 0.05$) indicating a clear dose related toxicity. On the other hand, the leaf extract appears to have been beneficial, with the low dose bringing the level back to the control level of 16.4±0.49 g/dL and the high dose increasing the level even more, to 16.7±0.47 g/dL.

This data indicates that RLD, especially at high doses is quite effective in maintaining haemoglobin levels whilst the RFD in higher doses could be seen as regressive in this aspect. The significant influence of plant extracts on haemoglobin levels in the context of anaemia treatment. Specifically, the leaves of certain plants can be quite effective in maintaining haemoglobin levels when administered at high doses. Furthermore, the flowers of these plants at elevated doses exhibit a regressive effect on haemoglobin levels (Coloraci *et al*., 2021).

The percentage lymphocyte levels, however, differed significantly among groups. The proportion of lymphocytes in the control group (I) was in the normal range (86.7±3.76), while in the AGS treated group (II) was slightly decreased (84±3.12) as a result of the immune suppressive action of the tumour stage. Upon giving the standard treatment drug the lymphocyte count reached 86.3±4.06 which was in line with that of the group I. The RFD extract at the lower dosage was able to maintain the lymphocyte level count at 86.3±4.1 while the higher dosage decreased the count a little to 83±2.52, but the effect was out of range which was an indicator of the dose dependent effect. More compelling was the observation that a low dose of the RLD extract produced a significantly increased number of lymphocytes (88.3±0.33), which hints at its potential to enhance the function of the immune system. On the contrary, a higher dose of the RLD extract caused a small decrease (84.3±3.18) though this was about the same range as in the group II.

Table 7. Haematological Parameters of C57BL/6 Mice Treatment with Docetaxel and *R. arboreum* DMSO RFD and RLD Extracts

Group	Group I	Group II	Group III	Group IV	Group V	Group VI	Group VII
RBCs ($X10^6/\mu L$)	5.85±0.46	6.22±0.33	5.9±0.26	5.83±0.18	5.52±0.51	6.29±0.049	6.16±0.23
WBCs ($X10^3/\mu L$)	11.9±0.78	12.9±0.66	13±1.77	9.77±0.58	10.4±0.77	10.4±1.19	11.7±0.89
Total Hemoglobin (g/dL)	16.4±0.35	13.4±0.34	14.7±0.56	13.8±1.57	12.7±0.69	16.4±0.49	16.7±0.47
Lymphocytes (%)	86.7±3.76	84±3.12	86.3±4.06	86.3±4.1	83±2.52	88.3±0.33	84.3±5.16

Values are expressed as mean ± SEM. Statistical significance (p) was calculated by one-way ANOVA followed by Dunnett's test (n=6), calculated by comparing treated groups with the control group (Group I)

Haematological parameter analysis is essential for evaluating physiological conditions and testing the effects of test substances (Etim *et al.*, 2014). In addition to toxicity associated with the test substances, these parameters can also indicate various diseases and conditions such as anaemia, leukaemia, inflammation, and infection (Paul *et al.*, 2017). The combined administration of RLD with RFD extracts along with docetaxel did not produce a notable variation in RBCs level when compared to the control groups (group I & II). Tests of lymphocyte numbers might indicate either an active infection since counts decrease or an inflammatory reaction when counts increase (Wang *et al.*, 2018).

The groups displayed equivalent haemoglobin concentration levels. The WBCs total counts frequently rise in connection to bacterial infections alongside inflammatory processes although they may flag up particular cancer or additional disease conditions (Syiman *et al.*, 2018). Lymphocytes along with monocytes, neutrophils plus eosinophils and basophils make up WBCs numbers while lymphocytes function as key cells in immune response (Elango *et al.*, 2018). The study by Wang *et al.*, (2018) found that an elevated total WBCs count before treatment proved to be an independent predictor for poor outcomes. This finding was validated through multivariate analysis. Neither surgery nor adjuvant chemotherapy affected the WBCs count, nor did the post-treatment ratio impact overall survival. Similarly, in the present study, the post-treatment WBCs count ratio did not affect overall survival in C57BL/6 mice. Additionally, lymphocyte percentage in the treatment groups (III-VII) did not significantly differ from the normal control groups (I & II).

4.12. Estimation of Serum Biochemical Parameters

The changes in biochemical parameters in the test groups were recorded after the treatment with RLD and RFD extracts, as well as docetaxel. The total protein levels in the experimental groups provide insight into overall physiological status, particularly tissue damage and inflammation. The lower total protein levels observed in the standard treatment (group III), RFD at high

dose (group V) and RLD at high dose (group VII) compared to both the control (group I) and AGS treated cancer groups (II) suggest that the group III, V & VII effectively inhibited the tumor progression.

This reduction indicates reduced systemic inflammation and tissue breakdown, as fewer proteins were released from damaged tissues into circulation (Wigertsad & Kaplan, 2023). In cancer conditions, inflammation and tissue degradation contribute to higher protein release; however, the observed decrease in protein levels in the treatment groups of III, V and VII (Table. 8) reflects improved tissue integrity and tumor suppression. The comparison between the treatment and cancer groups highlights the treatment interventions were successful in mitigating the adverse effects of tumor development.

SGOT (Serum Glutamic Oxaloacetic Transaminase) serves as a critical marker for liver and muscle health, as elevated levels are often indicative of cellular stress or tissue injury. In the standard treatment group (III), SGOT levels were significantly higher compared to all other groups, suggesting potential liver stress or hepatotoxicity induced by docetaxel. Side effects toward liver function were observed because of the drug's treatment which resulted in increased SGOT levels according to the findings of Putra *et al.*, 2021. The cancer treated in Group II, receiving the AGS cells showed increased SGOT levels because their tumours and inflamed tissue probably caused liver and tissue damage. The elevated SGOT levels detected in the group III (Table. 8) indicate a medicinal disadvantage against possible liver harm.

The liver enzyme marker known as Serum Glutamic Pyruvic Transaminase (SGPT) revealed both conditions of liver wellness and circumstances of liver stress and damage. The liver stress or damage from cancer cells created significant SGPT elevation in Group II models. The cancer burden generates hepatic inflammation which produces enzyme leakage from the liver along with hepatic dysfunction. Experimental findings demonstrate that group III experienced a significant reduction in SGPT levels thus indicating liver protection from docetaxel treatment according to Mahfudh *et al.*, (2021). The different impact of this drug becomes evident since the drug increases SGOT but decreases SGPT indicating its multifaceted effects on liver enzymes.

Different SGPT concentrations among the various therapeutic groups represent divergent treatment success and liver protection levels thus representing the crucial importance of medication dosage formulations together with their general therapeutic process. The treatment mechanism alongside the appropriate drug dosage determines both safety and effective results. Higher dose durations of treatment increase hepatotoxicity risks which cause the elevation of SGOT/SGPT levels (Sabiti & Sa'dyah, 2022).

Elevated ALP (Alkaline Phosphatase) levels are often associated with liver involvement, bone metabolism changes or tumor metastasis. In the context of gastric tumours, the liver may experience dysfunction due to metastasis or systemic inflammation, leading to increased ALP production. Additionally, changes in bone metabolism could occur in response to cancer progression. The elevated ALP levels observed in certain treatment groups IV and VI (low dose of flower and leaf) could suggest an adaptive response to treatment or residual liver and bone stress. Comparatively, groups with controlled ALP levels indicate less pronounced liver dysfunction and reduced systemic impact, reflecting improved therapeutic outcomes. ACP (acid phosphatase) serves as an indicator of cellular stress and is often elevated in conditions of inflammation, tumor burden or tissue breakdown.

In Group II, ACP levels were significantly elevated 27.7±4.33**, highlighting cellular stress and potential tissue damage induced by the cancer progression. ACP activity is linked to tumor burden and lysosomal enzyme release during cellular breakdown. In contrast, the Group III (standard treatment) and other treatment groups exhibited lower ACP levels, reflecting reduced cellular stress and improved tissue stability (Table. 8). The lower ACP levels 11.1±0.79 and 11.1±2.41 (group III and VII) suggest that the treatments were effective in minimizing cancer-related cellular damage. These results underscore the protective and inhibitory effects of the interventions on tumour progression and associated tissue damage. Liu *et al*., (2021) identified the potential anti-tumor effects of ACP-5862, indicated that it effectively minimized cancer-related cellular damage by significantly reducing cell proliferation and inducing apoptosis in ESCC (Esophageal Squamous Cell Carcinoma) cells.

Table 8. Effects of C57BL/6 Mice Treatment with Docetaxel and *R. arboreum* DMSO RFD and RLD Extracts

Group	Group I	Group II	Group III	Group IV	Group V	Group VI	Group VII
Total protein(mg/dl)	0.7±0.08	0.7±0.11	0.2±0.020*	0.7±0.10	0.6±0.08	0.6±0.06**	0.4±0.07
SGOT(U/L)	12±6.78	15±13.4*	87.5±0.318	14±1.21	17±9.73**	14±9.58	13±0.89
SGPT(U/L)	51.6±2.14	64.1±4.97*	24.2±0.779***	59.7±4.59	41.4±1.01	54.9±1.33	49.6±1.04
ALP (U/L)	8.33±14.4	15.4±28.6	11.1±19.3	19.9±34.4	12.4±21.5	34.1±59.1	9.8±17
ACP(U/L)	12.4±0.87	27.7±4.33**	11.1±0.79	19.2±2.45	13.4±2.74	12.8±2.12	11.1±2.41

Statistical significance (p) was calculated by one-way ANOVA followed by Dunnett's test (n=6); *p < 0.05, **p < 0.01, ***p < 0.001, calculated by comparing treated groups with the control group (Group I)

Serum SGOT, SGPT, ALP, and ACP enzyme activities are closely linked to liver injury (Lata *et al.*, 2014). SGOT and SGPT play key roles in cellular transamination processes crucial for protein metabolism in tumor tissue (Elango *et al.*, 2018). Elevated activities of these enzymes in the blood may stem from metabolic disruptions in normal cells and tumor-related disturbances.

When hepatocytes are damaged, their transport and membrane permeability are compromised, causing enzyme leakage (Kim *et al.*, 2009). The liver typically produces high concentrations of serum hepatobiliary enzymes like SGOT, SGPT, ALP and ACP (Sreelatha *et al.*, 2009). Damage to hepatocytes, such as necrosis or membrane damage, leads to increased serum enzyme levels as these enzymes are released into the bloodstream (Lata *et al.*, 2014).

The elevation in serum SGOT, SGPT, ALP and ACP activities in CPA (cyclophosphamide) -treated mice indicates liver cell damage. Lata *et al.*, (2014) found that *Phyllanthus fraternus* extract at doses of 200, 300 and 400 mg/kg body weight combined with CPA, dose-dependently reduced these enzyme levels, with significantly high protection was observed at 400 mg/kg.

The present study also shows that higher doses of *R. arboreum* extract (group V and VII) prevented AGS-induced liver damage effectively, whereas lower doses of *R. arboreum* extracts had minimal effects (Groups IV and

VI). Elevated serum SGOT, SGPT, ALP and ACP levels coupled with reduced levels in liver tissue are biochemical markers indicating tumor response. SGOT and SGPT play critical roles in cellular transamination processes essential for protein metabolism in tumor tissues. SGOT, SGPT, ACP and ALP activities lead to metabolic disruptions in normal cells and tumor-related changes, causing enzyme release into the bloodstream (Elango *et al*., 2018).

In the current study, higher levels of SGOT, SGPT, ACP and ALP were observed compared to group I & group II. ALT levels are established indicators of active disease and cancer risk, playing a crucial role in early cancer detection (Lorente *et al*., 1999; Vidya *et al*., 2022). Additionally, ALP specifically serves as a tumour marker for early cancer diagnosis.

4.13. Renal Function Parameters

The presence of urea, uric acid and creatinine in serum are markers of kidney dysfunction and indicate compromised membrane integrity due to free radicals (Table. 9). Treatment with RFD and RLD extracts, along with docetaxel at varying concentrations, conferred antioxidative efficacy. The urea, uric acid and creatinine levels across the experimental groups provide insights into kidney function and systemic physiological status. In group I (control), the urea level was 34.1±2.97 mg/dL, while group II showed a significant increase to 49.9±4.76 mg/dL, indicating impaired renal function due to tumor burden. Groups III (standard) 39±0.833 mg/dL, IV (RFD low dose) 31.4±0.775 mg/dL, V (RFD high dose) 29.8±0.769 mg/dL, VI (RLD low dose) 31.9±2.29 mg/dL and VII (RLD high dose) 26.7±1.17 mg/dL showed non-significant reductions, suggesting that the treatment interventions alleviated renal stress.

Uric acid levels in group I were 1.2±0.231 mg/dL, while group II exhibited a non-significant increase to 2.53±0.406 mg/dL, reflecting metabolic alterations associated with cancer progression. Groups III (1.93±0.467 mg/dL), IV (3.27±0.24 mg/dL), V (2.67±0.437 mg/dL), VI (2.07±0.897 mg/dL) and VII (2.27±0.769 mg/dL) displayed variable changes without significant deviations, indicating moderate effects of the treatments on uric acid metabolism. For creatinine, group I recorded 2.47±0.437 mg/dL, while group II (2.5±0.379 mg/dL) remained similar, showing no significant changes.

In contrast, groups III (0.933±0.24 mg/dL) and V (0.967±0.12 mg/dL) demonstrated significant reductions, highlighting improved renal function. Groups IV (3.13±0.353 mg/dL), VI (2.93±0.24 mg/dL) and VII (2.57±0.26 mg/dL) exhibited non-significant variations, indicating that the treatment efficacy varied among groups. These findings suggest that specific treatments were effective in reducing renal stress markers, while others displayed limited impact underscoring the importance of dose and therapeutic mechanisms in maintaining renal function.

Table 9. Renal Function Parameters of C57BL/6 Mice Treatment with Docetaxel and *R. arboreum* DMSO RFD and RLD Extracts

Group	Group I	Group II	Group III	Group IV	Group V	Group VI	Group VII
Urea (mg/dl)	34.1±2.97	48.9±4.76**	36±0.833**	31.4±0.775 ns	29.9±0.769 ns	31.9±2.29*	26.7±1.17**
Uric acid (mg/dl)	1.2±0.231	2.33±0.406 ns	1.93±0.467 *	3.27±0.24**	2.67±0.437 ns	2.07±0.897**	2.27±0.769 ns
Creatinine (mg/dl)	2.47±0.437	2.5±0.379**	0.933±0.24*	3.13±0.353 ns	0.967±0.12 *	2.93±0.24*	2.57±0.26**

Statistical significance (p) was calculated using one-way ANOVA followed by Dunnett's test (n=6). Results were considered non-significant (ns) if $p > 0.05$. * indicates $p < 0.05$. ** indicates $p < 0.01$.

Urea, creatinine, and uric acid are metabolic by products requiring filtration and excretion by the kidneys (Ezeugwunne *et al.*, 2017). Kidney malfunction results in their accumulation in the bloodstream (Du *et al.*, 2018). Administration of RLD and RFD extracts to C57BL/6 mice significantly elevated serum levels of urea, creatinine and uric acid. Elevated serum creatinine levels are a crucial indicator of renal failure, reflecting glomerular function status (Perrone *et al.*, 1992). Ezz *et al.*, (2011), also observed significantly elevated serum levels of uric acid, urea, and creatinine in a rat model of cisplatin-induced hepato and nephrotoxicity, against control group (I). The present study aligns with these findings, showing similar significant elevations in biochemical serum levels in treated groups (group III to VII) in comparison with the control group (group I). Elevated blood uric acid levels indicate hyperuricemia, a prognostic marker of inflammation (Jin *et al.*, 2012). RLD and RFD extracts of *R. arboreum* demonstrated significant improvement in renal function compared to C57BL/6

mice treated with docetaxel alone, as evidenced by serum levels of urea, creatinine and uric acid.

4.14. Determination of Enzymatic and Non- Enzymatic Antioxidant Markers

The protective effects of RLD and RFD extracts (100 and 200 mg/kg BW) against AGS-induced gastric cancer in C57BL/6 mice were investigated. The results indicated significant changes in oxidative stress markers, antioxidant enzyme activities and total protein levels across the groups, reflecting the physiological impact of cancer and the effects of treatments (Table. 10).

In group II, there is a marked increase in oxidative stress as evidenced by elevated SOD (0.62±0.03), catalase (0.60±0.01), GPx (0.24±0.01) and LPO (0.13±0.004) along with an increase in total protein levels (0.60±0.01). This is caused by cancer progression which generates excessive ROS leading to oxidative damage, lipid peroxidation and an upregulation of antioxidant enzymes in an attempt to counterbalance the oxidative stress.

In groups III to VII (treatment groups), there was significant reduction in oxidative stress markers like LPO and varying restoration of antioxidant enzyme activities (SOD, catalase and GPx) alongside decreased total protein levels compared to the group II. These suggest that the treatments exert a protective effect by reducing ROS, enhancing antioxidant defenses and mitigating oxidative damage. Among the treatment groups, group VI demonstrates notable improvements, particularly in catalase (0.45±0.08) and GPx (0.14±0.01), indicating its efficacy in restoring redox balance. The reduction in LPO levels across treatment groups reflects improved membrane stability and cellular integrity and enhancing antioxidant enzyme activity, with varying degrees of effectiveness.

Table 10. Determination of Total Protein, SOD, CAT, GPx, GSH and LPO in C57BL/6 Mice Treatment with Docetaxel and *R. arboreum* DMSO RFD and RLD Extracts

Group	Group I	Group II	Group III	Group IV	Group V	Group VI	Group VII
Total protein	0.40±0.01	0.60±0.01***	0.23±0.02***	0.29±0.009***	0.25±0.01***	0.24±0.001***	0.18±0.002***
SOD	0.40±0.01	0.82±0.03***	0.40±0.01ns	0.51±0.06**	0.39±0.04ns	0.56±0.05*	0.42±0.06*
Catalase	0.23±0.005	0.60±0.01***	0.24±0.04ns	0.31±0.01**	0.36±0.006*	0.43±0.08*	0.36±0.03*
GPx	0.09±0.003	0.24±0.01***	0.08±0.001ns	0.10±0.01**	0.08±0.002ns	0.14±0.01**	0.13±0.04**
GSH	0.24±0.01	0.33±0.006	0.14±0.03	0.22±0.04	0.2±0.009	0.21±0.05	0.17±0.01
LPO	0.04±0.004	0.13±0.004*	0.04±0.01ns	0.09±0.01**	0.08±0.001*	0.11±0.04*	0.08±0.01*

Statistical significance (p) was calculated by one-way ANOVA followed by Dunnett's test (n=6); ns - non-significant, *p < 0.05, ***p < 0.001.

Lipid peroxidation (LPO) is a significant contributor to biological harm, propagated by free radical reactions (Gaschler and Stockwell, 2017). It damages cells by extracting hydrogen atoms from polyunsaturated fatty acids (PUFAs) in membrane lipids, altering membrane fluidity and potential ultimately leading to cell dysfunction and death (Niki, 2009; Wiktorowska *et al.*, 2015). Elevated LPO levels indicate oxidative damage and the generation of free radicals (Seckin *et al.*, 1993).

Antioxidants are crucial in protecting against such damage caused by ROS (He *et al.*, 2017). The antioxidant system operates through three lines of defense. The first line includes preventive antioxidants like SOD, CAT, GPx and nonenzymatic molecules that neutralize $O_2^{\cdot}$, break down H_2O_2 and bind metal ions (Leyon and Kuttan, 2004). Odabasoglu *et al.* (2006) observed lower SOD, GPx, and GSH levels and higher CAT and LPO levels in rats treated with indomethacin compared to healthy controls. Similarly, the present study also found lower SOD, GPx and GSH levels in Groups IV to VII of C57BL/6 mice compared to Group I, with higher CAT and LPO levels observed in treated groups compared to control groups.

4.15. Myeloperoxidase (MPO) Activity

In this study, the activity of myeloperoxidase (MPO) in whole blood was found to be significantly higher in Group I than in treatment groups (Table. 11).

except for Groups IV, VI and VII. It is important to note that the increased basal neutrophil MPO activity is not related to soluble plasma MPO, as it reflects intracellular MPO activity. The myeloperoxidase (MPO) activity levels across the groups show significant variation, reflecting the extent of inflammation and the effects of treatment interventions. In group II, MPO activity is significantly elevated (0.45±0.078), indicating increased neutrophil infiltration and inflammation due to cancer progression. This rise in MPO is caused by the tumor microenvironment, which triggers immune responses and the generation of ROS, contributing to oxidative damage.

In the treatment groups (groups III to VII), MPO activity decreases compared to group II, indicating a reduction in inflammation. Groups III, V, VI and VII show MPO levels close to the control (group I, 0.22±0.021), suggesting a partial to substantial anti-inflammatory effect of the treatments. Group IV shows a moderate reduction in MPO (0.31±0.059), suggesting some inflammation persists. Among the treatment groups, group V (0.20±0.005) and group VII (0.23±0.018) (Table. 11) exhibit MPO levels closest to the control group, indicating these treatments were the most effective in suppressing inflammation. Treatment interventions reduce MPO levels to varying extents, suggesting their role in mitigating cancer induced inflammatory responses.

Table 11. Estimation of Myeloperoxidase of C57BL/6 Mice Treatment with Docetaxel and *R. arboreum* DMSO RFD and RLD Extracts

Group	Group I	Group II	Group III	Group IV	Group V	Group VI	Group VII
MPO (mg protein)	0.22±0.021	0.45±0.078*	0.21±0.033ns	0.31±0.059*	0.20±0.005ns	0.25±0.036*	0.25±0.018*

Statistical significance (p) was calculated by one-way ANOVA followed by Dunnett's test (n=6), ns - non-significant, *p < 0.05, calculated by comparing treated groups with the control group (I).

MPO is a crucial enzyme in neutrophils, involved in generating oxidative bursts that kill bacteria (Hirche *et al*., 2005). Neutrophils produce O_2^- through oxygen reduction using NADPH, leading to H_2O_2 formation and reactive microbicidal oxidants; during sepsis, neutrophils use MPO to produce antimicrobial oxidants (Hsu *et al*., 2008). In this study, C57BL/6 mice in group II, carrying AGS cells, showed higher bacterial density and neutrophil infiltration

in the antrum compared to groups I and III to VII. This highlights MPO as a critical factor influencing bacterial density and neutrophil infiltration severity. MPO contributes to innate immune response by catalysing the formation of strong oxidant like hypochlorous acid, effectively targeting pathogens also MPO activity during neutrophil activation is essential for immune response, deficiencies in MPO leads to increased infections and its role in regulating both neutrophil response and bacterial load in tissues (Lin et al., 2024).

4.16. Histopathological Analysis

Histopathological analysis of the group I showed a normal gastroesophageal junction with non-neoplastic gastric foveolar and squamous epithelium, appearing consistent and unremarkable across stomach layers (Figure. 24). No pathological changes or abnormalities were observed in group I. In contrast, stomach specimens from group II revealed lesions lined by low-grade neoplastic columnar epithelium with gastric glands containing paneth and goblet cells (Figure. 24). Group III displayed a gastroesophageal junction with non-neoplastic gastric columnar lining epithelium and an edematous submucosa underlying the gastric epithelium in microscopic analysis (Figure. 24). In Group IV and Group V treated groups, microscopic analysis showed a gastroesophageal junction with non-neoplastic gastric columnar lining epithelium (Figure. 25). Group VI and Group VII exhibited non-neoplastic gastric foveolar epithelium thrown into folds and lined by columnar epithelium, suggesting a complete response to treatment (Figure. 26).

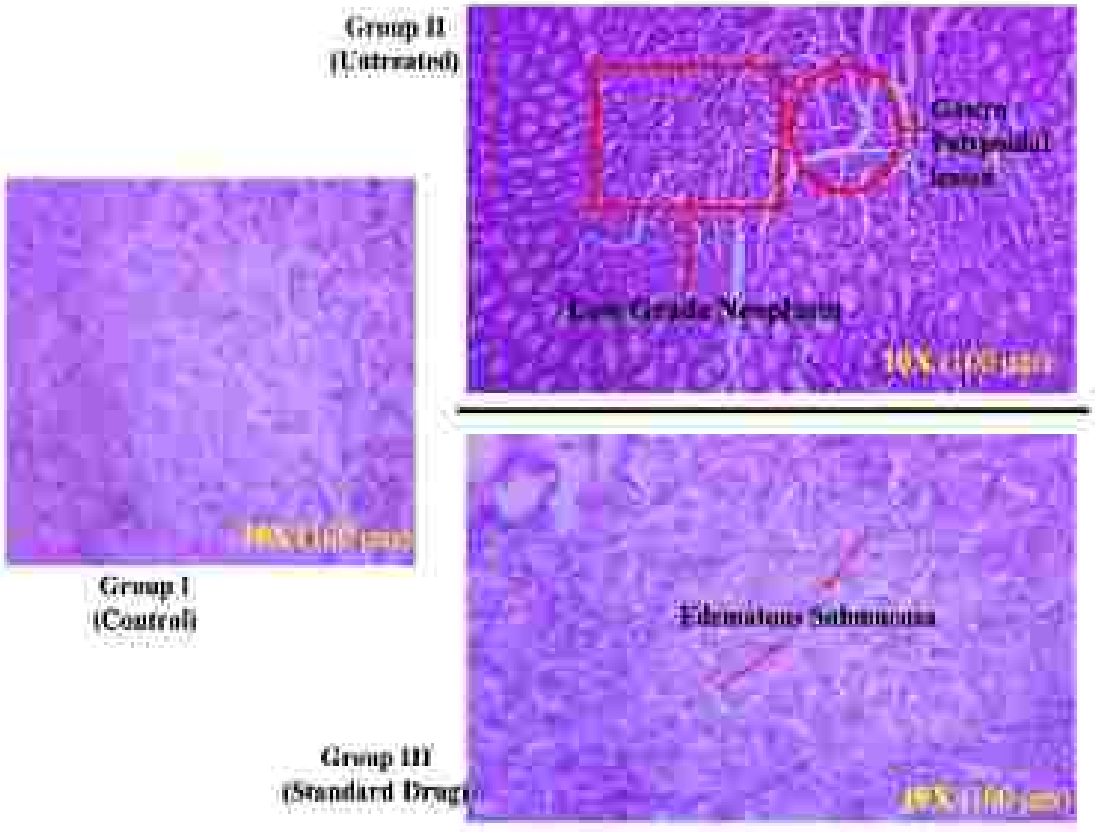

Figure 24. The Microscopic Examination of Stomach Specimens from Different Treatment Groups Provides Valuable Insights into the Cellular Changes Induced by Various Therapeutic Interventions. Group I- (control group) 10X shows normal squamous epithelium; Group II- (AGS) 10X shows gastric mucosa with low-grade neoplastic cells; Group III- 10X shows non neoplastic cells with edematous submucosa.

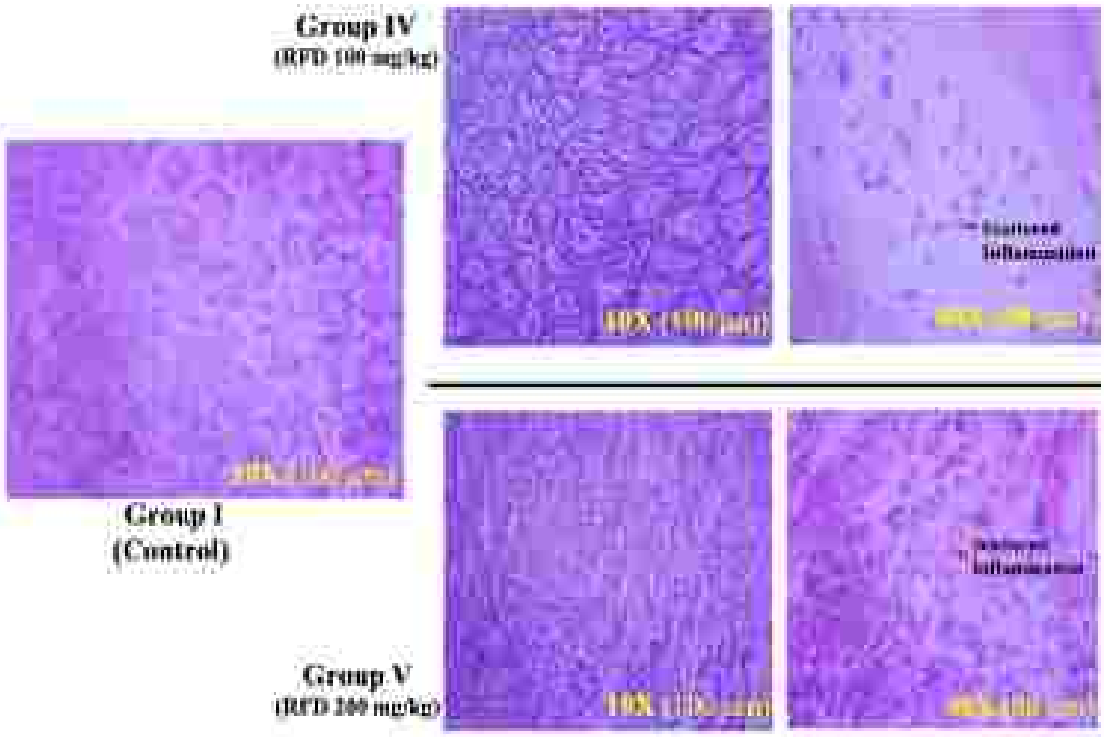

Figure 25. The Microscopic Observation of Histopathological Examination of C57BL/6 (Stomach) Treated with Flower Extracts

Histopathological examination of gastric malignancy in the mouse model, both the low and high dose RFD extract treated groups exhibited limited immune cell infiltration. Scattered inflammatory cells, including lymphocytes, macrophages and neutrophils were sparsely distributed within the tumor microenvironment. The present observation indicates that the immune response to the tumour was subdued, regardless of the flower extract dose (Figure. 25). The lack of significant immune cell accumulation suggests that the RFD extract, at both low and high concentrations, may not have strongly influenced immune activation or modulation of tumour-associated inflammation. According to Nowarski *et al.*, (2013) the accumulation of immune cells or tumor-associated inflammation plays a crucial role. The study emphasizes that a lack of immune cell accumulation can impact the immune activation or modulation to tumour related inflammation.

This could imply either a limited immunomodulatory capacity of the extract or a more localized, subtle effect that may not fully translate into strong immune engagement in this model.

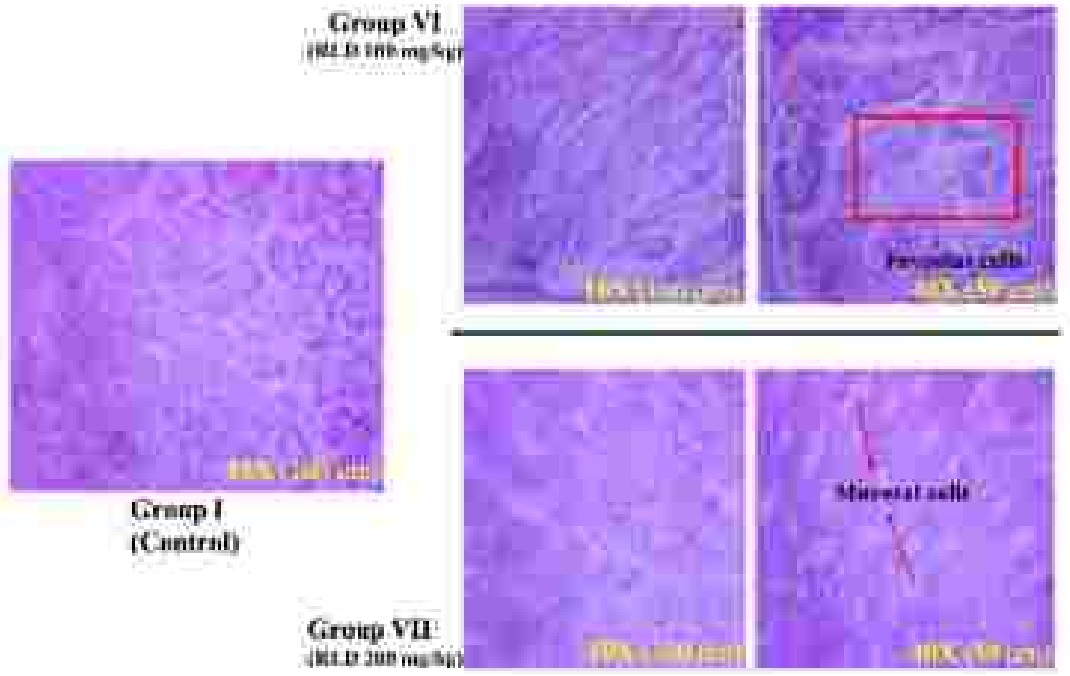

Figure 26. The Microscopic Observation of Histopathological Examination of C57BL/6 (Stomach) Treated with Leaf Extracts

Histopathological examination of gastric malignancy in the mice model, both the low and high-dose RLD extract treated groups (VI & VII) showed a complete response to the therapy. The gastric tissue exhibited the presence of well-organized foveolar and mucosal cells, which are critical components of the gastric lining responsible for secreting protective mucus (Figure. 26). This restoration of normal cellular architecture suggests that the leaf extract not only inhibited tumour growth but also promoted the regeneration of healthy gastric epithelium. The presence of these cells indicates effective healing and a re-establishment of normal gastric function, highlighting the leaf extract's potent therapeutic potential in reversing tumor-associated damage.

Prostaglandins protect the gastric mucosa and epithelial cell proliferation is crucial for ulcer crater re-epithelialization (Fornai *et al*., 2011). Gastric carcinoma shows architectural and cytologic heterogeneity often with mixed histologic elements (Shin and Park, 2024). Historically, gastric carcinoma classification has relied on Lauren's criteria which categorizes it into intestinal type, diffuse type adenocarcinoma and less commonly an indeterminate type (Hu *et al*., 2012). Günes *et al*., 2018 studied carvacrol's effects on human gastric adenocarcinomas (AGS) and normal human

fibroblasts (WS-1). They administered carvacrol orally to Wistar rats at 100 mg/kg BW, observing increased oxidative stress in stomach tissues and blood compared to controls. Necropsy revealed pathological changes like gas-filled stomachs, bowels and swollen abdomen contributing to increased body weight in the experimental group.

In the present study, histopathological examination of AGS-induced gastric lesions (group II) revealed extensive damage to the gastric mucosa with edema and leukocyte infiltration in the submucosal layer accompanied by increased body weight. However, C57BL/6 mice treated with docetaxel and RLD and RFD extracts showed better protection of the gastric mucosa. Histopathological analysis confirmed significant differences between control and experimental groups (I), with the extracts demonstrating dose-dependent cytoprotective effects such as reduced ulcer area, decreased submucosal edema and less leukocyte infiltration. The extracts also flattened mucosal folds, potentially contributing to gastroprotective effects by reducing gastric motility and protecting against gastric irritants (Garrick *et al.*, 1986; Takeuchi and Nobuhara, 1985) at a dosage of 200 mg/kg BW combined with AGS induction, varying degrees of tumour development were observed.

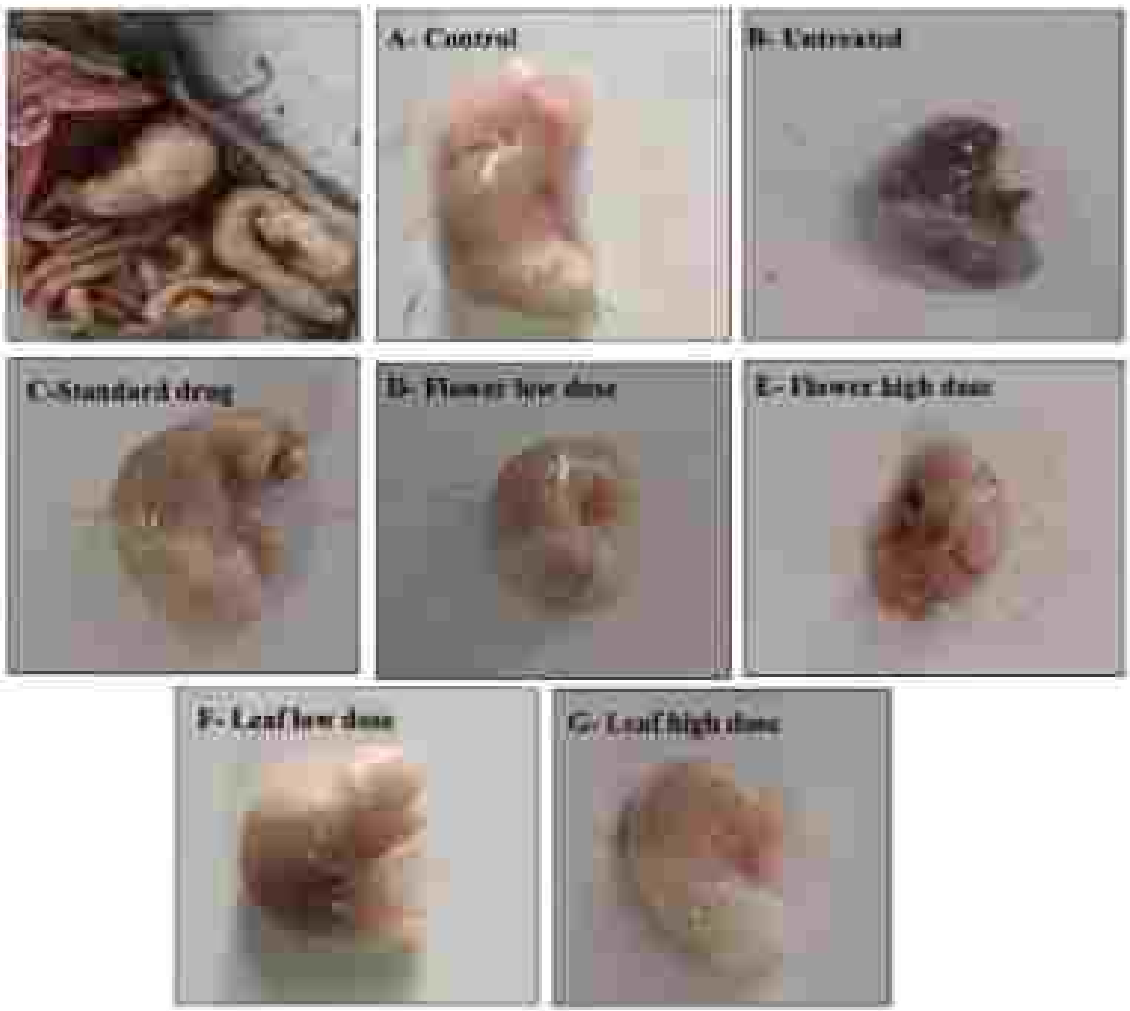

Figure 27. A Representative Example of Tumour Development Derived from Different Groups of C57BL/6 Mice. **(A)** Displays the stomach of the control group (I) with no tumours. **(B)** Exhibits an AGS-induced stomach without treatment (group II), showing tumour formation. **(C)** the stomach of mice treated with the docetaxel alongside AGS induction (group III). **(D)** and **(E)** depict the stomachs of mice treated with low dose (group IV) and high dose (group V) of RFD extract and **(F)** and **(G)** depicts the stomachs of mice low dose (group VI) and high dose (group VII) of RLD extracts.

4.17. *In silico* ADME Studies by SwissADME

4.17.1. SwissADME

The drug likenesses of selected phytoconstituents were ascertained by evaluating the physicochemical and pharmacokinetic properties using SwissADME. XlogP3 computes the lipophilicity of a molecule and represents partition coefficient values (logarithm) of compounds in the n-octanol/water system. The properties provide insights into the pharmacokinetic properties of

the compounds and were checked using Discovery Studio's built in ADMET protocol. The various parameters tested in this study were aqueous solubility, Blood Brain Barrier (BBB) level, Absorption level and CYPD26. It is an important parameter and affects bioavailability, membrane permeability, distribution and clearance route of drugs. This parameter also plays an essential role in pharmacological and toxic properties of drugs. XlogP3 values for the quercetin and 2,3,4,6-tetramethoxystyrene compounds were within the required limit below five. The polar surface area of the compound is in an inverse relationship with human intestinal absorption. Usually most of the drugs must not pass the blood brain barrier if the target is not related to the nervous system. The total numbers of rotatable bonds are 1-7, which shows the flexibility of all the selected compounds. All the compounds were obeying Lipinski rule of five.

Table 12. Molecular Properties of Selected Compounds from *R. arboreum* Leaf and Flower

Name of the compound	Canonical SMILES	Formula	Molecular weight	nrtob	H-bond acceptors	H-bond donors	Molar refractivity	TPSA
Quercetin	C1=CC(=C(C=C1C2=C(C(=O)C3=C(C=C(C=C3O2)O)O)O)O)O	$C_{15}H_{10}O_7$	302.24 g/mol	1	7	5	78.03	131.36 Å²
gamma-sitosterol	CC[C@@H](CC[C@@H](C)[C@H]1CC[C@@H]2[C@@]1(CC[C@H]3[C@H]2CC=C4[C@@]3(CC[C@@H](C4)O)C)C)C(C)C	$C_{29}H_{50}O$	414.71 g/mol	6	1	1	133.23	20.23 Å²
alpha-amyrin	C[C@@H]1CC[C@@]2(CC[C@@]3(C(=CC[C@H]4[C@]3(CC[C@@H]5[C@@]4(CC[C@@H](C5(C)C)O)C)C)C)[C@@H]2[C@H]1C)C)C	$C_{30}H_{50}O$	426.72 g/mol	0	1	1	135.14	20.23 Å²
2,3,4,6-tetramethoxystyrene	COC1=CC(=C(C(=C1C=C)OC)OC)OC	$C_{12}H_{16}O_4$	224.25 g/mol	5	4	0	62.50	36.92 Å²
beta-sitosterol	CCC(C(C)C)CCC(C1CCC2C1(C)CCC1C2CC=C2C1(C)CCC(C2)O)C	$C_{29}H_{50}O$	414.71 g/mol	6	1	1	133.23	20.23 Å²
LIMITS	-	-	**>500**	**>20**	**>10**	**>5**	**40-130**	**20-200**

A super family gene member of human cytochrome P450 enzyme is a versatile one and could metabolize the various hydrophobic compounds through its oxidation and eventually remove the foreign compounds. Among this major family of CYPs, the three isoforms viz. 2D6, 2C9 and 3A4 have been considered more important and responsible for microsomal oxidation of most of the drugs in humans. CYP2D6 metabolizes more than 27.5 % of drugs and is extensively considered as polymorphic drug-metabolizing enzyme isoform that could catalyze the bio-conversion of many xenobiotics. Owing to this reason, the present study has chosen this isoform to predict the ADME property of the synthesized compounds. However, all the compounds had been predicted as non-inhibitors of CYP2D6 except for the quercetin that had drug-like properties.

Table 13. Pharmacokinetic Properties of Selected Compounds from *R.arboreum* Leaf and Flower

Name of the compound	XLOGP3	ESOL: Class	GIA	BBB Permeation	CYP2D6 inhibitor	Lipinski violation	PAINS alert	Synthetic Accessibility
Quercetin	1.54	-3.16	High	No	Yes	Yes; 0 violation	1 alert: catechol_A	3.23
gamma-sitosterol	9.34	-7.90	Low	No	No	Yes; 1 violation: MLOGP>4.15	0 alert	6.30
alpha-amyrin	9.01	-9.16	Low	No	No	Yes; 1 violation: MLOGP>4.15	0 alert	6.17
2,3,4,5-tetramethoxystyrene	2.75	-2.80	High	Yes	No	Yes; 0 violation	0 alert	2.22
beta-sitosterol	9.34	-7.90	Low	No	No	Yes; 1violation: MLOGP>4.15	0 alert	6.30
LIMITS	**-0.7 to 5**	-	-	-	-	**0 to 1**		**0 to 10**

GIA- Gastro Intestinal Absorption, BBB- Blood Brain Barrier

4.17.2. Chemical Structure and Bioavailability Radar

The Bioavailability Radar is displayed for a rapid appraisal of drug-likeness. Six physicochemical properties were taken into account: lipophilicity, size, polarity, solubility, flexibility and saturation. A physicochemical range on each axis was defined by descriptors adapted from refs and depicted as a pink area in which the radar plot of the molecule has to fall entirely to be considered drug-like. The pink area represents the optimal range for each properties (lipophilicity: XLOGP3 between –0.7 and +5.0, size: MW between 150 and 500 g/mol, polarity: TPSA between 20 and 130 Å2, solubility: log S not higher than 6, saturation: fraction of carbons in the sp3 hybridization not less than 0.25 and flexibility: no more than 9 rotatable bonds) (Table. 14). Except for the gamma-sitosterol, alpha-amyrin and beta-sitosterol all the compounds are in good bioavailability radar.

Table 14. Results of Biological Radar for Selected Compounds

S. No.	Name of the Compounds	Biological Radar
1	Quercetin	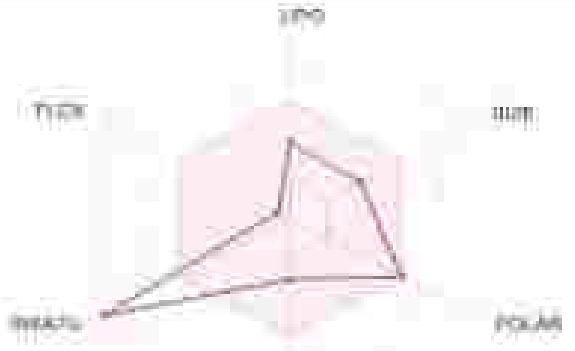
2	gamma-sitosterol	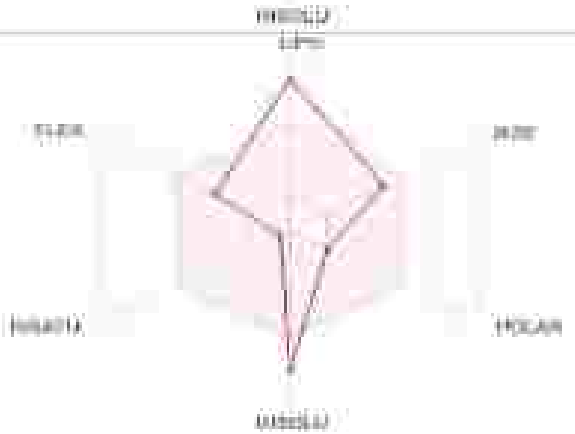

3	alpha-amyrin	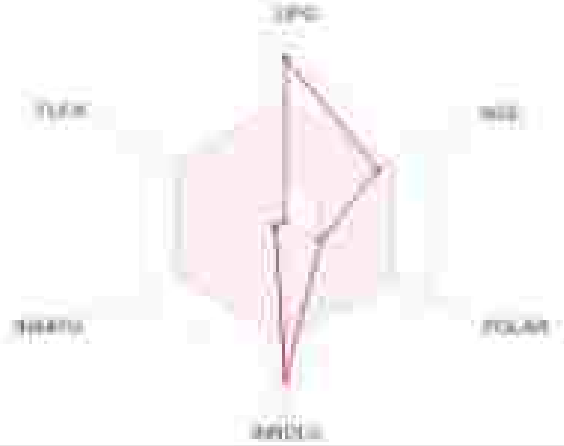
4	2,3,4,6-tetramethoxystyrene	
5	beta-sitosterol	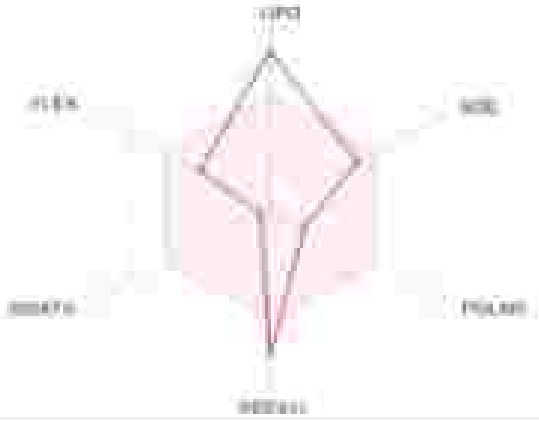

4.18. Network Pharmacology

4.18.1. Compound Identification and Target Screening

After excluding compounds without known targets, 10 key chemical compounds were identified from the leaves and flowers of *R. arboreum* using GC-MS data and the IMPPAT database. The targets for these compounds were obtained from the BindingDB database. Significant compounds which were identified included beta-sitosterol, quercetin and 2,3,4,6-tetramethoxystyrene. These targets were mapped to human genes by

inputting them into the UniProt database with the species option set to *Homo sapiens*. Additionally, 955 gastric cancer-related targets were identified from the GeneCards database (Figure. 28). By comparing the predicted candidate targets of *R. arboreum* with these gastric cancer-related targets, 113 unique targets of *R. arboreum* against gastric cancer were identified. Of these, 22 genes were found to be common between the disease and the plant constituents and these were selected for further study.

Figure 28. Venn Diagram intersecting the Common Targets for Gastric Cancer and *R. arboreum* (Leaf and Flower)

4.18.2. PPI Network Construction and Key Gene Identification

The STRING tool was utilized to construct a protein-protein interaction (PPI) network for the compound-disease-target relationships associated with *R. arboreum*. This analysis focused on 22 overlapping targets with a confidence score threshold set at >0.7. The resulting PPI network comprised 22 nodes and 101 edges, with an average node degree of 9.18 and an average local clustering coefficient of 0.685. The PPI network was analyzed for the top ten compound-disease-targets based on betweenness, closeness and degree centrality metrics.

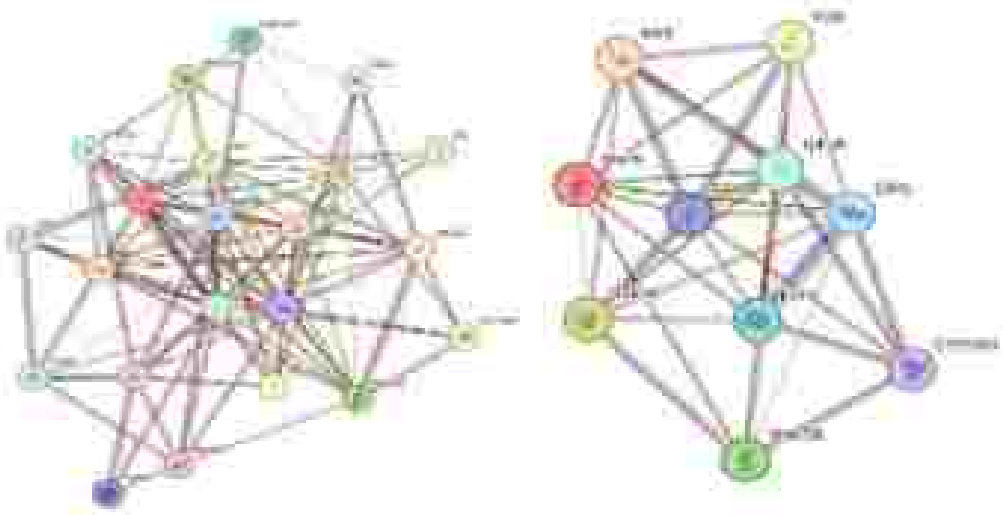

Figure 29. Protein-Protein Interaction **(A)** 22 Overlapping Targets of Gastric Cancer and *R. arboreum* **(B)** Top Ten Compound-Disease-Targets.

4.18.3. Visualization of Drug-Target Interactions Using Cytoscape

Cytoscape 3.6.1 software was used to visualize the scored targets obtained from the STRING database analysis, highlighting the interactions between *R. arboreum* and gastric cancer (Figure. 30). This visual representation was designed to clearly illustrate the relationships between the identified compounds and their corresponding targets associated with gastric cancer. The network consisted of 10 nodes and 35 edges with an average node degree of 7 and an average local clustering coefficient of 0.81. To enhance clarity and interpretability the node attributes were customized with adjustments made to both the colour and size of the nodes. This approach effectively depicted the drug-target interactions, highlighting key nodes that represent significant compounds or targets. As a result, it provided a detailed and informative visualization of the drug-disease interactions, providing a foundation for further analysis of the pharmacological potential of *R. arboreum* against gastric cancer.

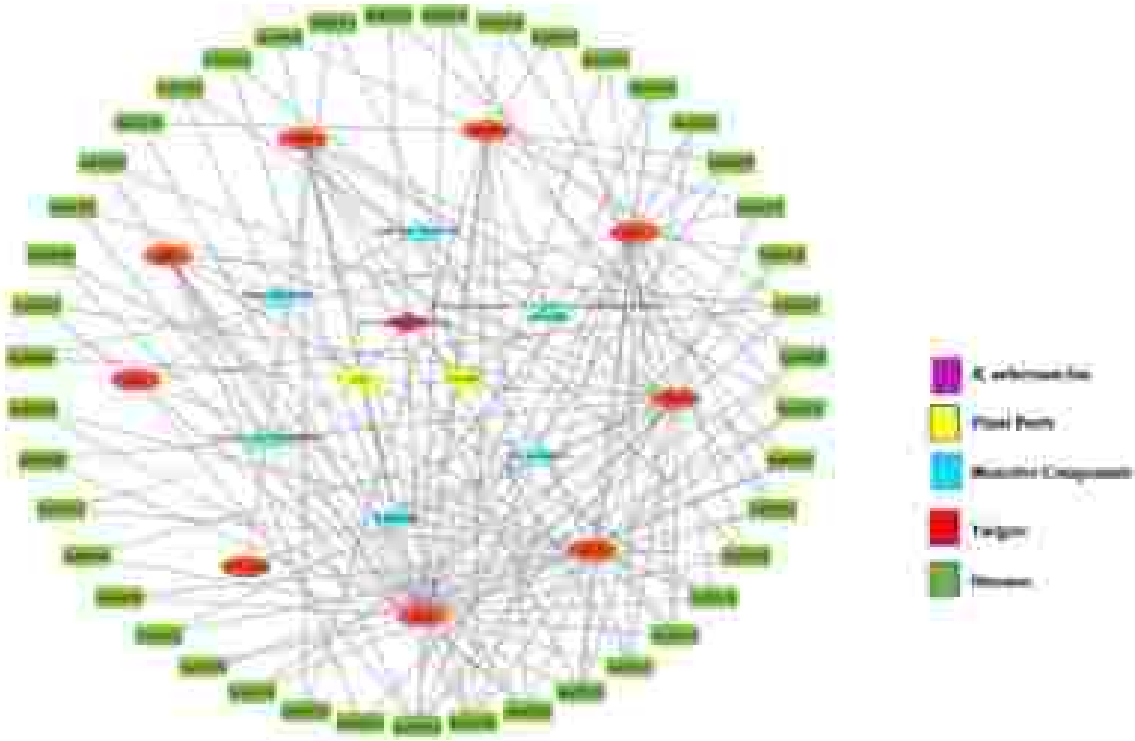

Figure 30. Integrated Network of Protein-Drug Interactions for *R. arboreum* with Gastric Cancer and Associated Diseases

In the present study, 10 key chemical compounds were identified from the leaves and flowers of *R. arboreum* using GC-MS data and the IMPPAT database. These compounds, including significant ones such as beta-sitosterol and quercetin, were mapped to their respective human gene targets via the UniProt database. A total of 933 gastric cancer-related targets were obtained from the GeneCards database. Chen *et al*., 2024, assessed the network pharmacology and molecular docking methods to explore potential mechanisms for the Tiao-Yuan-Tong-Wei decoction (TYTW) in the treatment of gastric cancer and key targets discovered in consonance with pathways relevant to gastric cancer include ESR1 and PTGS2 among those identified. The presence of common targets in the findings of the study indicates that TYTW and *R. arboreum* exerts their therapeutic effects against gastric cancer through molecular mechanisms at an overlap. The fact that targets such as ESR1 are common among them puts these compounds in a position to activate important pathways involved in cancer metastasis.

Yang *et al*., 2020 constructed a protein-protein interaction (PPI) network for 15 quercetin-related targets using the STRING tool. Their study emphasized

systematic visualization and measurement of protein functions in cellular contexts. The PPI network determined that AKT1 was the pivotal protein, having the highest degree of interaction followed by other notable proteins like EGFR, SRC and IGF1R. Six hub targets with high degrees of interactions were revealed through the CytoHubba analysis to be AKT1, EGFR, SRC, IGF1R, PTK2 and KDR which play crucial roles in gastric cancer progression. The present study also constructed a PPI network using the STRING tool for *R. arboreum* with an emphasis on compound-disease-target relationships. Resulted in 22 overlapping targets with a confidence score threshold greater than 0.7. The resultant PPI network had well-connected average metrics: it included 22 nodes and 101 edges. Further analyses were done by Cytoscape to illuminate interactions between *R. arboreum* and gastric cancer by centrality measures among the top ten compound-disease-targets networks representing their connections adapted to exhibit as informative and detailed visualization as possible about drug-disease interactions. The approaches are very similar among them concerning their application of centrality metrics in determining significant targets found within PPI networks.

4.18.4. Functional Enrichment and Pathway Analysis of *R. arboreum* in Gastric Cancer

The study identified multiple mechanisms through which *R. arboreum* may act against gastric cancer by using the bioinformatics tool ShinyGO 0.80. This analysis revealed 20 enriched Gene Ontology (GO) terms, each with a statistical significance of $P < 0.05$, indicating a strong association with the biological processes related to gastric cancer. The GO terms were categorized into three main areas (Udhaya *et al.*, 2020):

1. Biological Processes: These refer to the various biological activities and pathways that the plant compounds may influence within the cancer cells. This could include processes like apoptosis (programmed cell death), cell proliferation and immune response, all of which are crucial in cancer development and treatment.

2. Cellular Components: This category identifies the specific parts of the cell where the plant's compounds may exert their effects. It helps to pinpoint whether these compounds target the cell membrane, nucleus, mitochondria or

other cellular structures providing insights into how they may disrupt cancer cell function.

3. Molecular Functions: These are the specific biochemical activities that the compounds from *R. arboreum* might affect. For example, this could include binding to certain proteins, inhibiting enzymes or interacting with DNA which could help to inhibit cancer growth or promote cancer cell death.

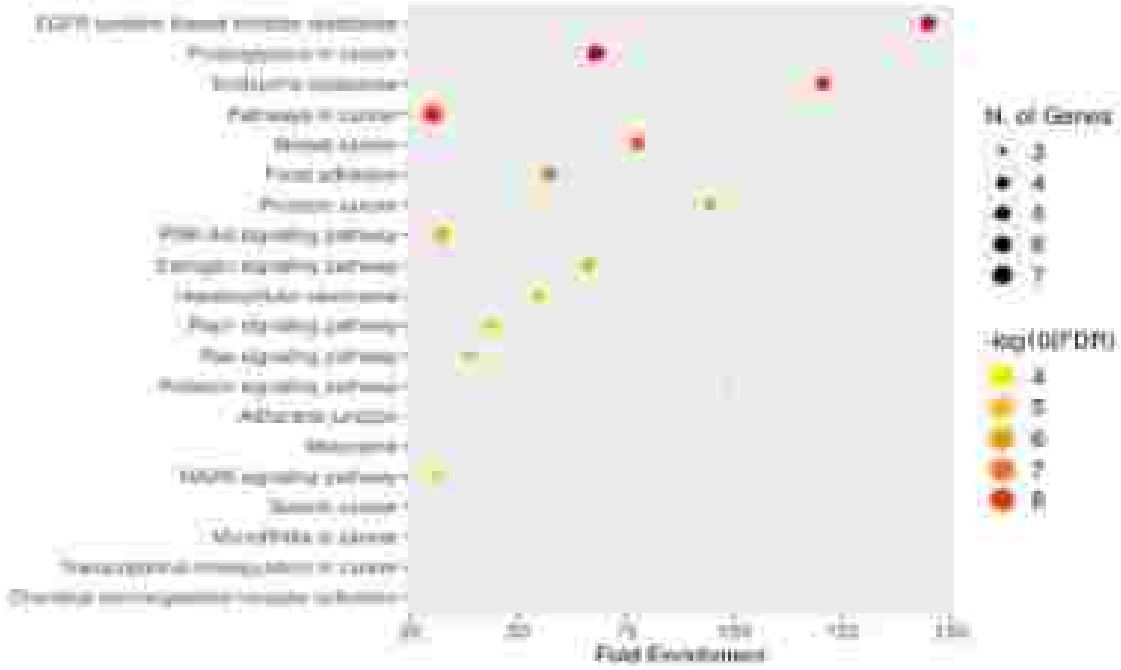

Figure 31. GO Enrichment Analysis for Targets across Different Modules

Gene Ontology enrichment analysis shows the significant thresholds set at p-value < 0.01 and FDR < 0.01. In the resulting plot, the y-axis represents significantly enriched GO terms and the x-axis shows the different modules. The size of each dot reflects the rich factor which is the ratio of target genes associated with a specific GO term to the total number of annotated genes within that term. A larger rich factor indicates a higher level of enrichment.

The above pathway enrichment analysis revealed the key genes like EGFR, GSK3B, IGF1R, KDR, MET, ESR1, ESR2 and MMP9 are significantly involved in multiple cancer-related pathways. For instance, the EGFR tyrosine kinase inhibitor resistance pathway (Path:hsa01521) has a fold enrichment of 144.82 and an FDR of 5.42E-09, indicating a strong over representation. Similarly, the endocrine resistance pathway (Path:hsa01522) shows a fold enrichment of 120.43 with an FDR of 9.26E-09. Other notable pathways include

gastric cancer (Path:hsa05226) with a fold enrichment of 46.38 and an FDR of 0.00018287 and the broadly encompassing pathways in cancer (Path:hsa05200) with a fold enrichment of 30.22 and an FDR of 9.81E-09. These values underscore the significant role these genes play in cancer progression, treatment resistance and signaling mechanisms. Although *HMGCR* is not highlighted in these results because they didn't appear prominently in the specific pathway enrichment results, still it remains an important gene to consider, particularly in pathways related to lipid metabolism and cholesterol biosynthesis, which can influence cancer development and progression.

4.18.4.1. KEGG Path Enrichment Analysis

KEGG pathway enrichment analysis identified the top 20 pathways ($p < 0.05$, Figure 32 and Table 15), which included EGFR Tyrosine Kinase Inhibitor Resistance and Pathways in Cancer. The specific regulatory targets within these pathways are detailed in Figures 32 a and 32 b. The KEGG pathway maps highlight the most relevant regulatory targets, which include ESR1, GSK3B, ESR2, CYP19A1, MET, HMGCR, KDR, IGF1R, MMP9 and EGFR.

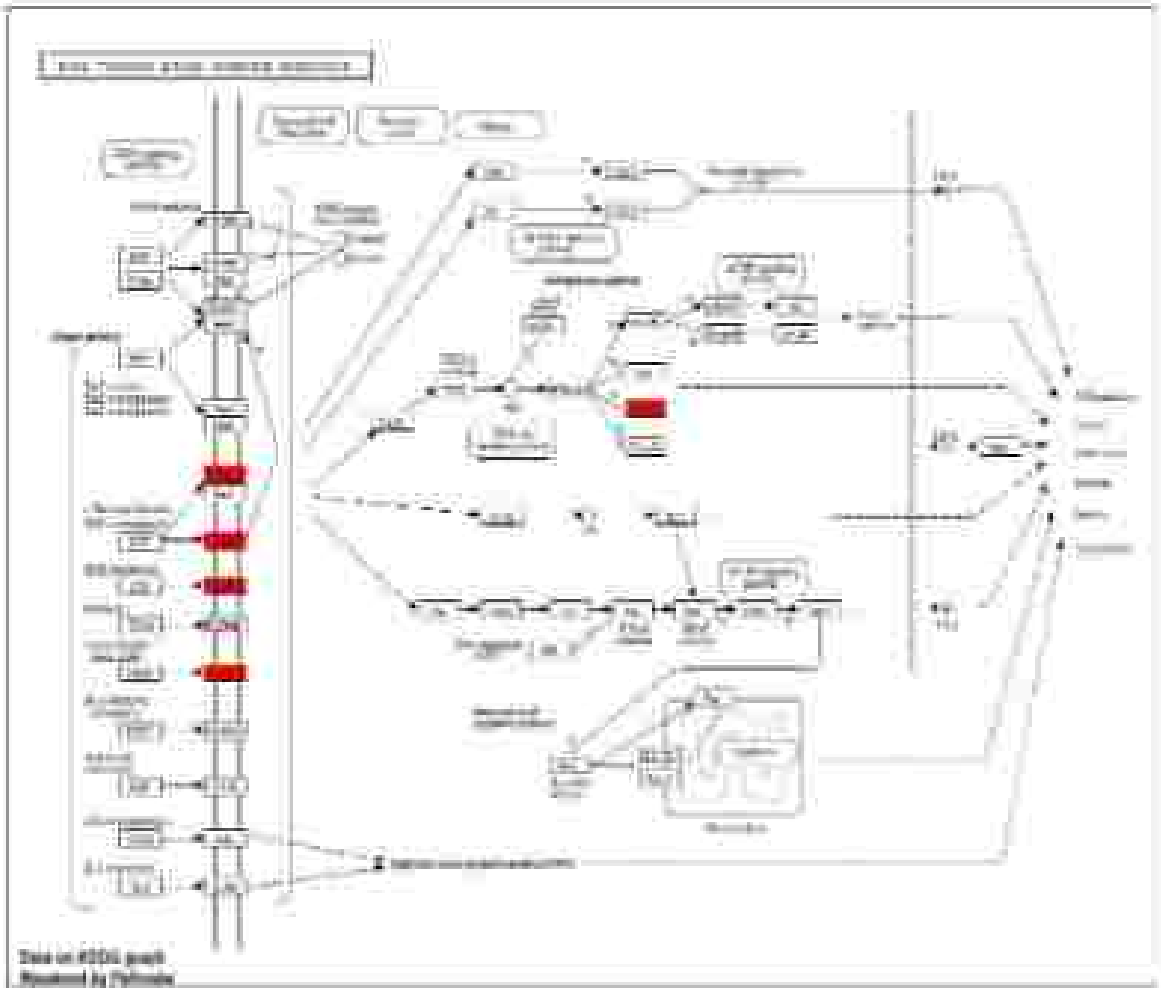

Figure 32. a: The Simplified KEGG Pathway for Gastric Cancer (Hsa05226) is shown, with Red-Coloured Nodes Representing the Targets Identified in the Modules. (*The original image is sourced from the KEGG database*).

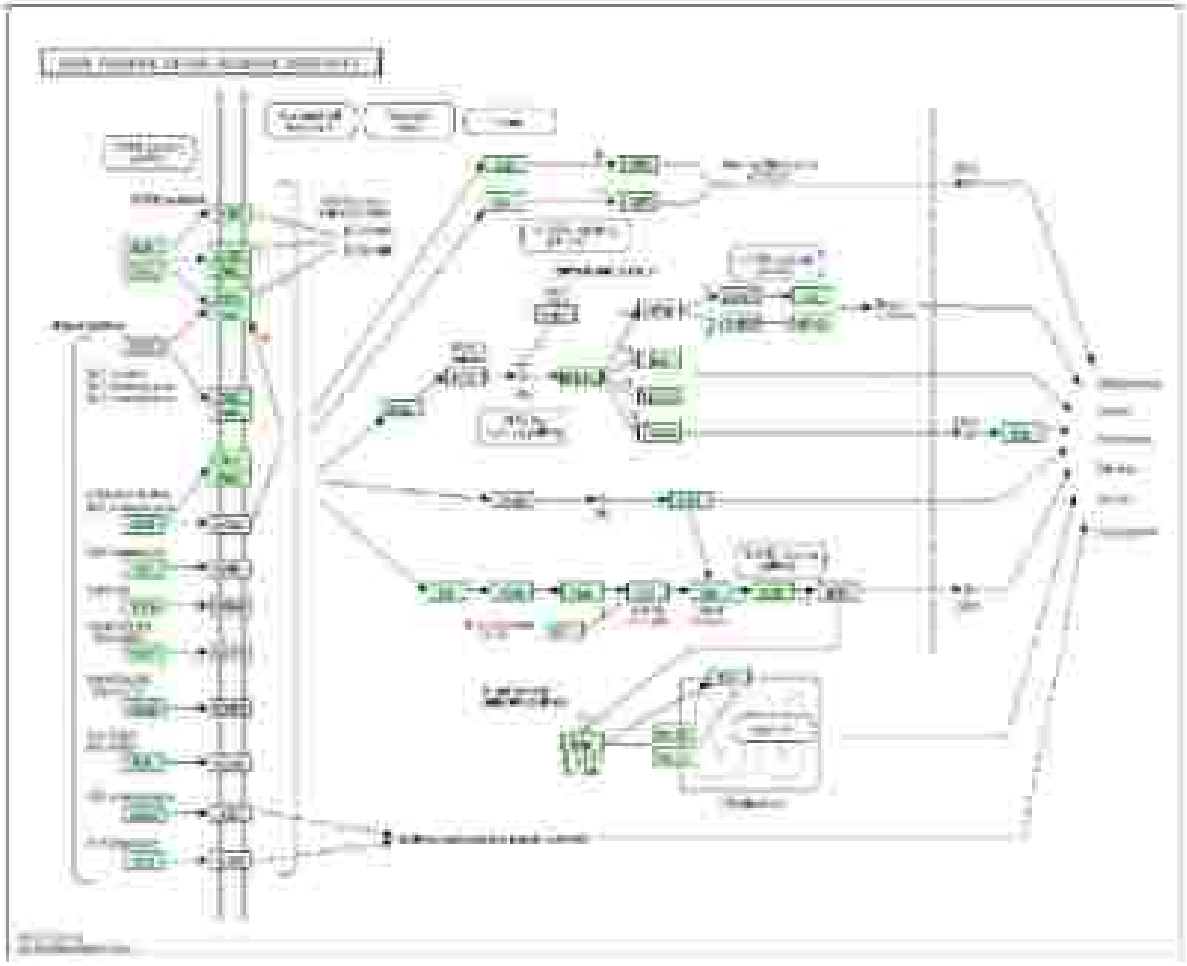

Figure 32. b: The Simplified KEGG Pathway for Gastric Cancer (Hsa05226) is shown, with Green-Coloured Nodes Representing the Potential Targets Identified in the Modules. *(The original image is sourced from the KEGG database).*

Table 15. KEGG Enrichment Analysis (top 20): Functional Insights into Biological Processes

Enrichment FDR	nGenes	Pathway Genes	Fold Enrichment	Pathway	Genes
5.42E-09	5	79	144.8184456	Path:hsa01521 EGFR tyrosine kinase inhibitor resistance	EGFR GSK3B IGF1R KDR MET
9.26E-09	5	96	120.4295516	Path:hsa01522 Endocrine resistance	EGFR ESR1 ESR2 IGF1R MMP9
2.38E-05	3	70	98.06814268	Path:hsa04917 Prolactin signaling pathway	ESR1 ESR2 GSK3B
2.38E-05	3	71	96.6802817	Path:hsa04520 Adherens junction	EGFR IGF1R MET
2.38E-05	3	72	95.3373	Path:hsa05218 Melanoma	EGFR IGF1R MET
9.02E-07	4	97	94.36486392	Path:hsa05215 Prostate cancer	EGFR GSK3B IGF1R MMP9
5.07E-06	5	147	77.82663306	Path:hsa05224 Breast cancer	EGFR ESR1 ESR2 GSK3B IGF1R
5.42E-09	6	202	67.98333663	Path:hsa05205 Proteoglycans in cancer	EGFR ESR1 IGF1R KDR MET MMP9
2.90E-06	4	138	66.3217391	Path:hsa04915 Estrogen signaling pathway	EGFR ESR1 ESR2 MMP9
1.99E-07	5	200	57.2023	Path:hsa04510 Focal adhesion	EGFR GSK3B IGF1R KDR MET
5.61E-06	4	167	54.8047904	Path:hsa05225 Hepatocellular carcinoma	EGFR GSK3B IGF1R MET
0.000016267	3	148	46.38004054	Path:hsa05226 Gastric cancer	EGFR GSK3B MET
1.27E-05	4	210	43.5828571	Path:hsa04015 Rap1 signaling pathway	EGFR IGF1R KDR MET
0.00022204	3	161	42.6354037	Path:hsa05206 MicroRNAs in cancer	EGFR MET MMP9
1.83E-05	4	235	38.946383	Path:hsa04014 Ras signaling pathway	EGFR IGF1R KDR MET
0.00036083	3	183	35.5863212	Path:hsa05202 Transcriptional	IGF1R MET MMP9

				misregulation in cancer	
0.00038432	3	197	34.8441624	Path:hsa05207 Chemical carcinogenesis - receptor activation	EGFR ESR1 ESR2
2.57E-06	5	354	32.5177966	Path:hsa04151 PI3K-Akt signaling pathway	EGFR GSK3B IGF1R KDR MET
3.93E-05	4	294	31.1306122	Path:hsa04010 MAPK signaling pathway	EGFR IGF1R KDR MET
9.81E-09	7	530	30.2201887	Path:hsa05200 Pathways in cancer	EGFR ESR1 ESR2 GSK3B IGF1R MET MMP9

The epidermal growth factor (EGF) receptor family is an important subgroup of receptor tyrosine kinases functioning in cellular communication and regulation. The receptors are activated by the binding of the extracellular EGF and then they dimerize, meaning that two receptor molecules pair up. This leads to the second event: autophosphorylation-were the receptor preferably adds phosphate groups to its cytosolic domains. The phosphorylated domains become docking sites for other intracellular proteins, extending the signal transduction cascade into the cell.

The EGF receptors activate several key intracellular pathways, including the PI3K/AKT pathway which promotes cell survival and growth. The MAPK pathway which regulates cell proliferation, differentiation and migration (Stefani *et al.*, 2021; Chen *et al.*, 2022; He *et al.*, 2021). These pathways collectively drive essential cellular processes such as growth, proliferation, differentiation, migration and survival. However, in many tumours, receptors from the EGF receptor family become dysregulated, leading to excessive signaling and uncontrolled cell growth (Hassanein *et al.*, 2021). A well-known example is the receptor erbB-2 (HER2) which is overexpressed in many cancer cases, making it a significant target for cancer therapies (Yoon & Oh, 2024). The understanding of this receptor family's role in both normal cellular functions and cancer has led to the development of targeted therapies that inhibit

overactive receptors, thereby slowing down or halting tumour growth (Dembic, 2020).

In the study, KEGG enrichment analysis of the Pathways in Cancer was conducted to identify key molecular pathways involved in gastric cancer progression. This analysis highlighted critical processes such as cell cycle regulation, apoptosis and angiogenesis, revealing their significant association with the gene sets derived from present data (Arya *et al.*, 2021). The enriched pathways, supported by statistical measures like p-values and FDR, underscore their potential role in tumor development (Elasbali *et al.*, 2024). The pathway enrichment analysis revealed significant involvement of key genes like EGFR, GSK3B, IGF1R, KDR, MET, ESR1, ESR2 and MMP9 in critical cancer-related pathways. For example, the EGFR tyrosine kinase inhibitor resistance pathway showed a fold enrichment of 144.82 with an FDR of 5.42E-09, highlighting its role in treatment resistance. While the broader pathways in cancer category had a fold enrichment of 30.22 and an FDR of 9.81E-09. These values underscore the critical roles these genes play in cancer progression and resistance. Visualizing these pathways provided insights into the molecular mechanisms at play, offering valuable information for identifying potential therapeutic targets and guiding future research in gastric cancer treatment (Islam *et al.*, 2022).

The present study highlights quercetin's binding affinities with several key proteins, including ESR1, GSK3B, KDR, MMP9 and EGFR all of which are involved in various gastric cancer pathways. Both studies underscore the importance of targeting these critical proteins to inhibit cancer progression with CHE and quercetin emerging as promising therapeutic agents.

4.19. Molecular Docking using Schrodinger

The molecular docking study evaluated the binding affinities of five compounds- beta-sitosterol, quercetin, gamma-sitosterol, alpha-amyrin and 2,3,4,6-tetramethoxystyrene against four key target proteins (PDB IDs: 1B3D, 1ERR, 6GQ0 and 6S9B). The results revealed that quercetin demonstrated the highest binding affinities among all tested proteins. The binding energies were -8.68 kcal/mol for 1B3D, -6.407 kcal/mol for 6S9B, -6.053 kcal/mol for

6GG0 and -5.374 kcal/mol for 1ERR. Additionally, the docking conformations of the most relevant targets with regulatory roles, identified through KEGG analysis such as ESR1, KDR, MMP9 and EGFR were also evaluated. These findings highlight quercetin, found in both the leaves and flowers of *R. arboreum* as a promising candidate for further exploration due to its strong interaction with these critical proteins.

Table 16. The Binding Energies of Top 4 Key Target Proteins with Top 5 Compounds: Molecular Interaction and Stability

Target	PDB ID	Ligand	Docking score : Kcal/mol	Docetaxel Standard Drug
MMP	1B3D	Quercetin	-8.68	
		gamma-sitosterol	-4.53	-5.318
		beta-sitosterol	-4.36	
		2,3,4,6-tetramethoxystyrene	-4.23	
		alpha-amyrin	-3.56	
EGFR	6G96	Quercetin	-6.40	-3.783
		2,3,4,6-tetramethoxystyrene	-3.29	
		beta-sitosterol	-2.67	
		gamma-sitosterol	-1.91	
		alpha-amyrin	-1.16	
KDR	6GQ9	Quercetin	-6.05	-6.623
		gamma-sitosterol	-3.06	
		beta-sitosterol	-3.04	
		alpha-amyrin	-3.01	
		2,3,4,6-tetramethoxystyrene	-2.44	
ESR1	1ERR	Quercetin	-5.57	-5.698
		2,3,4,6-tetramethoxystyrene	-3.28	
		beta-sitosterol	-3.05	
		alpha-amyrin	-2.62	
		gamma-sitosterol	-2.52	

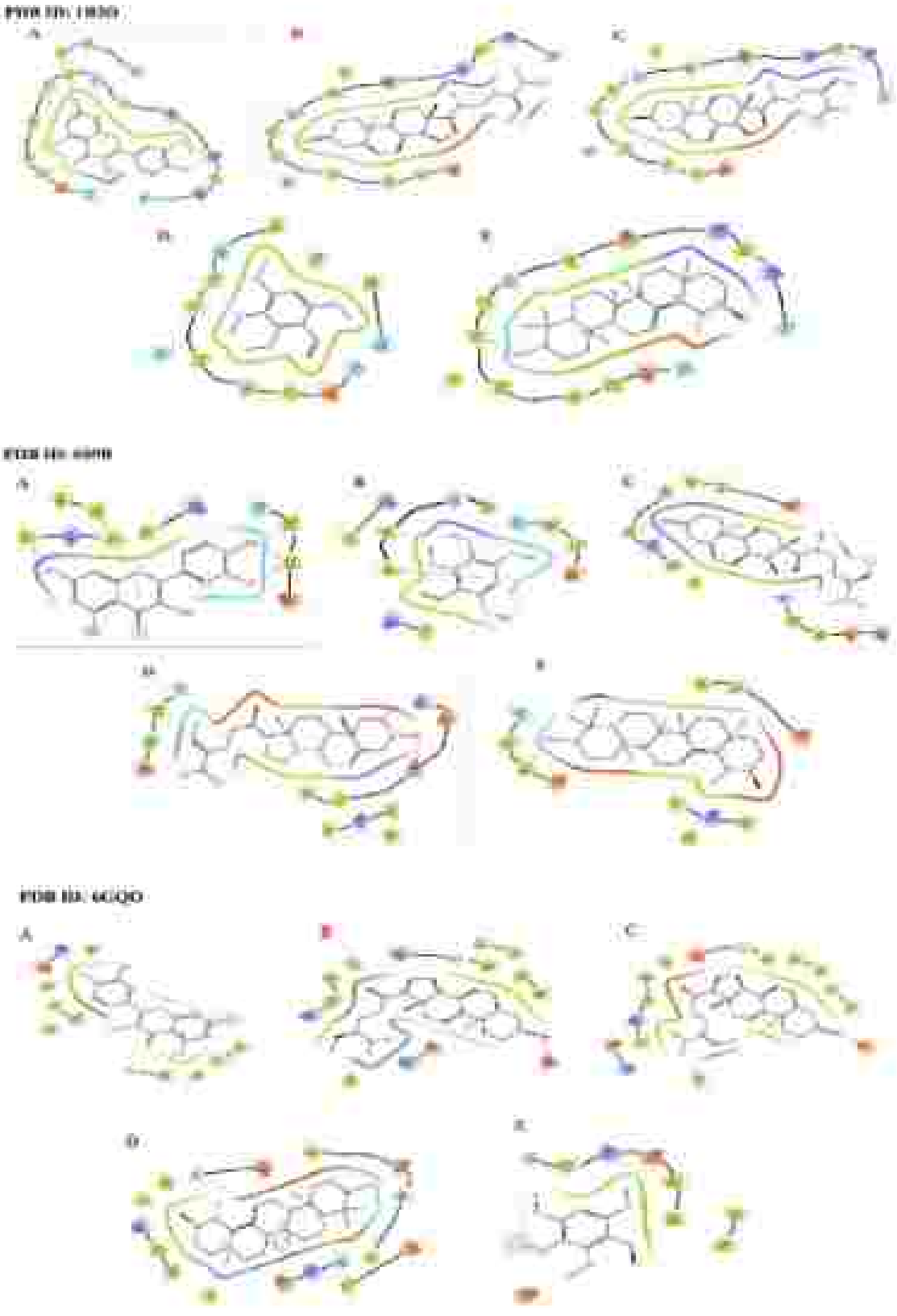

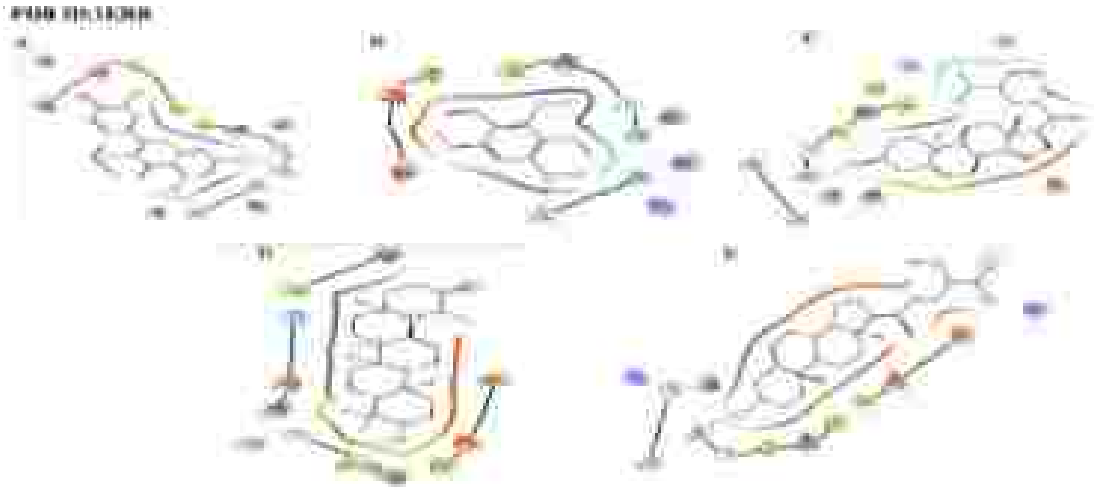

Figure 33. 2D Structure of PDB ID- 1B3D (**A-** Quercetin, **B-** gamma-sitosterol, **C-** beta-sitosterol, **D-** 2,3,4,6-tetramethoxystyrene, **E-** alpha-amyrin), **PDB ID- 6S9B** (**A-** Quercetin, **B-** 2,3,4,6 tetramethoxystyrene, **C-** beta-sitosterol, **D-** gamma-sitosterol, **E-** alpha-amyrin). PDB ID- 6GQ0 (**A-** Quercetin, **B-** gamma-sitosterol, **C-** beta-sitosterol, **D-** alpha-amyrin, **E-** 2,3,4,6-tetramethoxystyrene). **PDB ID- 1ERR** (**A-** Quercetin, **B-** 2,3,4,6-tetramethoxystyrene, **C-** beta-sitosterol, **D-** alpha-amyrin, **E-** gamma-sitosterol).

Similarly, Guo *et al*., 2024, demonstrated that quercetin, luteolin and Oleanin interact with key targets in gastric cancer cells particularly EGFR and MAPK1. Quercetin exhibited strong binding to EGFR with a score of –8.3, suggesting its potential to modulate EGFR and MAPK1 levels and inhibit gastric cancer progression. This aligns with the present study, which also found strong binding affinities for quercetin.

Additionally, Chowdhury *et al*., 2023, reported quercetin's high binding affinity to the dopamine D2 receptor, potentially aiding in managing emesis from gastric cancer treatments. Quercetin's gastroprotective effects, including reducing gastric mucosal injury and oxidative damage, highlight its broad therapeutic potential in gastric cancer emphasizing the need for further research into its mechanisms and clinical applications.

EGFR overexpression has been associated with poor prognosis in gastric cancer with 2-35% of cases showing protein overexpression or gene amplification. Multiple clinical trials evaluating EGFR inhibitors in gastric cancer have yielded disappointing results, largely due to lack of patient selection

based on EGFR status. However, recent studies targeting EGFR amplifications detected in circulating tumor DNA have shown promise with response rates around 55% in some patients. Ongoing trials are now focusing on EGFR-positive gastric cancers selected by genomic or proteomic biomarkers. Future directions involve utilizing next-generation sequencing, ctDNA analysis and artificial intelligence to better identify and target EGFR alterations potentially improving survival outcomes in gastric cancer patients (Adashek *et al*., 2020).

MMP9 (Matrix Metalloproteinase 9) plays a crucial role in cancer progression by facilitating tumor invasion, metastasis and angiogenesis through the degradation of the extracellular matrix (ECM). Inhibiting MMP9 is considered a potential therapeutic strategy as it can limit the invasive capabilities of cancer cells and disrupt the formation of new blood vessels, thereby starving tumours of necessary nutrients. Additionally, MMP9 influences the immune microenvironment and its inhibition may enhance anti-tumor immune responses. Recent advancements have led to the development of therapeutic antibodies such as andecaliximab which specifically target MMP9 and are currently in clinical trials, offering a more selective approach compared to traditional small-molecule inhibitors. The dual role of MMP9 which can also exhibit tumour-suppressive effects in certain contexts (Augoff *et al*., 2022). Dong *et al*., 2020, studied USP19 (ubiquitin-specific peptidase 19) for enhancing MMP2/MMP9-mediated tumorigenesis in gastric cancer and reported MMP9 to play a significant role in gastric cancer progression and metastasis. MMP9 is important in regulating cell migration and invasion through digesting the extracellular matrix. Studies showed that MMP9 enzyme activity was associated with increased cancer cell migration and invasion capabilities. Bioinformatics analysis of gastric cancer datasets revealed MMP9 mRNA levels were associated with more aggressive disease. These findings report MMP9 as a potential therapeutic target and prognostic marker for gastric cancer.

The expression of KDR, also referred to as VEGF receptor-2, is vital for malignant angiogenesis in gastric cancer (GC). In GC, high KDR expression is

considered a specific feature and thus a possible target for GC therapy. The formation of the molecular docking analysis between quercetin and KDR (VEGF receptor-2) remained promising. Quercetin showed good binding energy of KDR, Vina score -9.4 assessing the possibility of interaction at a greater strength. The docking simulation exhibited a large binding cavity on KDR with dimensions of 31 x 21 x 17 Å, providing ample space for quercetin to dock essentially. The center of this binding site was put at coordinates 2, 22, 122 inside the KDR protein structure. These docking results suggest that quercetin would be able to modulate activity in KDR related to gastric cancer and other angiogenic processes (Yang *et al.*, 2020).

Estrogen receptor 1 (ESR1) acts as a tumor suppressor in gastric cancer (GC). In a study conducted by Shang *et al.*, 2024, it was found that exosomes secreted by cancer-associated fibroblasts (CAFs) promote GC cell viability, migration and invasion by upregulating interleukin-32 (IL32) and downregulating ESR1 expression. The interaction between IL32 and ESR1 was evaluated using co-immunoprecipitation and dual-luciferase reporter assays, indicating that increased levels of IL32 negatively regulate ESR1 levels. This suggests that the IL32/ESR1 axis plays a significant role in the progression of gastric cancer, highlighting the potential of targeting CAF-derived exosomes for therapeutic strategies in metastatic GC.

4.19.1. Molecular Docking with Standard Drug- Docetaxel

Docetaxel, a chemotherapeutic agent belonging to the taxane family, has emerged as a significant treatment option for gastric cancer, particularly in advanced and metastatic stages. It functions by disrupting microtubule dynamics during cell division thereby inhibiting mitosis and inducing apoptosis in rapidly dividing cancer cells. Its efficacy in gastric cancer is often explored in combination with other chemotherapeutic agents such as cisplatin and 5-fluorouracil, enhancing therapeutic outcomes. Despite its effectiveness in tumor suppression, docetaxel is associated with a range of side effects including neutropenia, fatigue and gastrointestinal toxicity which may limit its use in certain patient populations. Nevertheless, docetaxel remains a foundation in the systemic treatment of gastric cancer contributing to

improved survival rates and quality of life in patients, particularly in those who are resistant to first-line therapies. Its role continues to be refined through ongoing clinical trials aimed at optimizing dosage regimens and minimizing adverse effects.

In this study, molecular docking of docetaxel was performed with key gastric cancer-related proteins including MMP9, EGFR, KDR and ESR1 to assess its binding affinities. These proteins play critical roles in tumor invasion, angiogenesis and progression. The docking results were compared to the binding affinities of bioactive ligands from *R. arboreum* extracts (leaf and flower). By evaluating the interactions of docetaxel with these target proteins, the study aimed to determine its potential efficacy relative to the natural compounds providing insights into the therapeutic value and mechanism of both docetaxel and the *R. arboreum* ligands in inhibiting gastric cancer pathways.

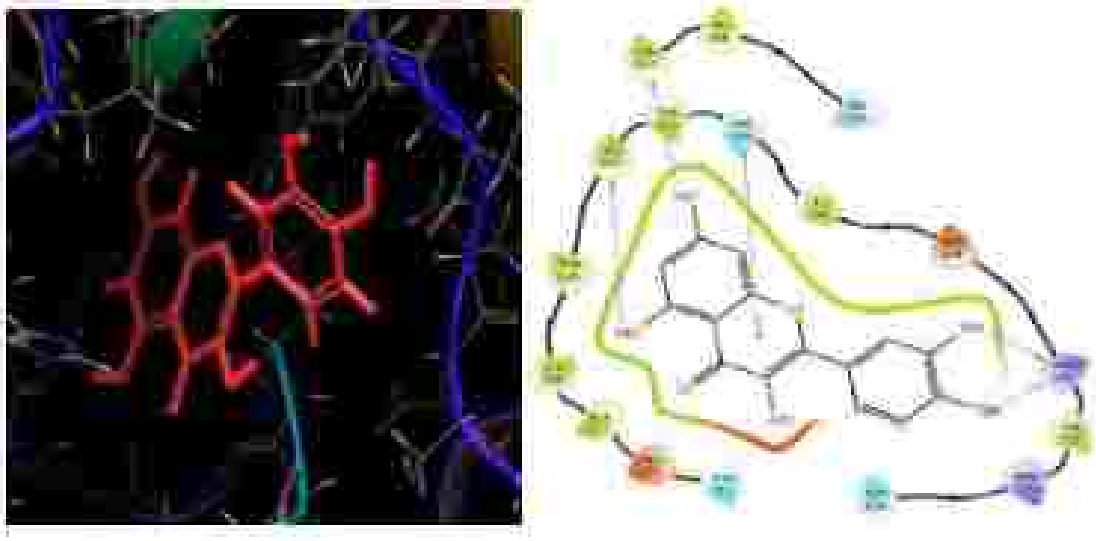

Figure 34. 3D and 2D Structure of Quercetin (MMP9)

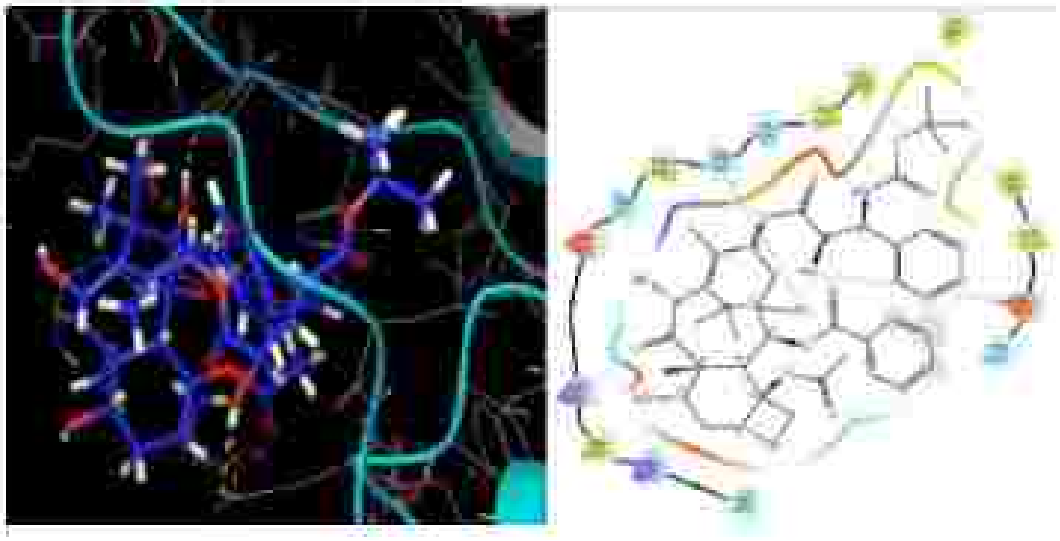

Figure 34.a. 3D and 2D Structure of Docetaxel

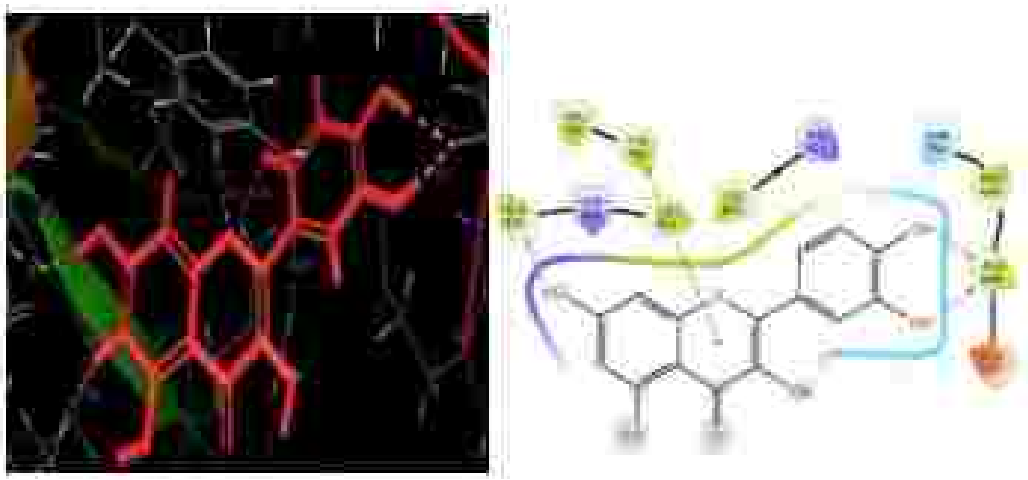

Figure 35. 3D and 2D Structure of Quercetin (EGFR)

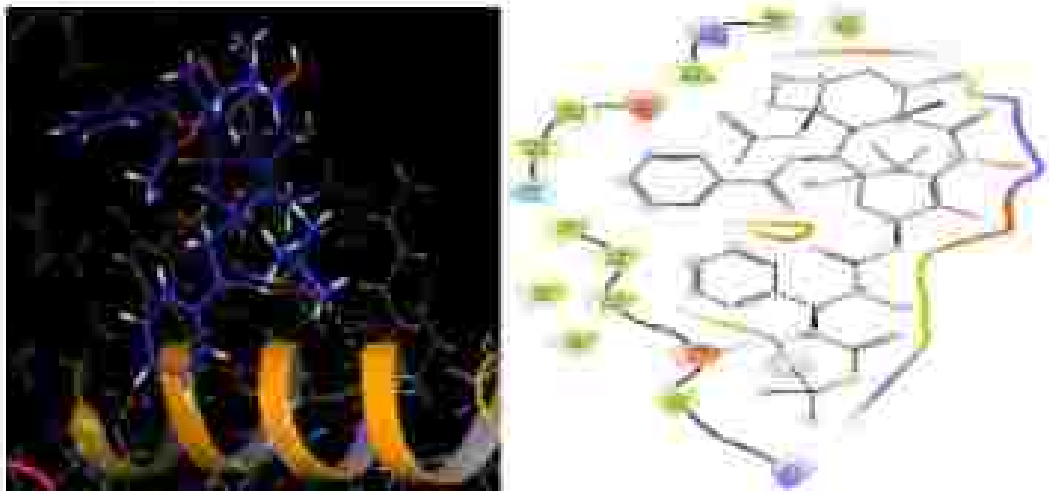

Figure 35. a. 3D and 2D Structure of Docetaxel

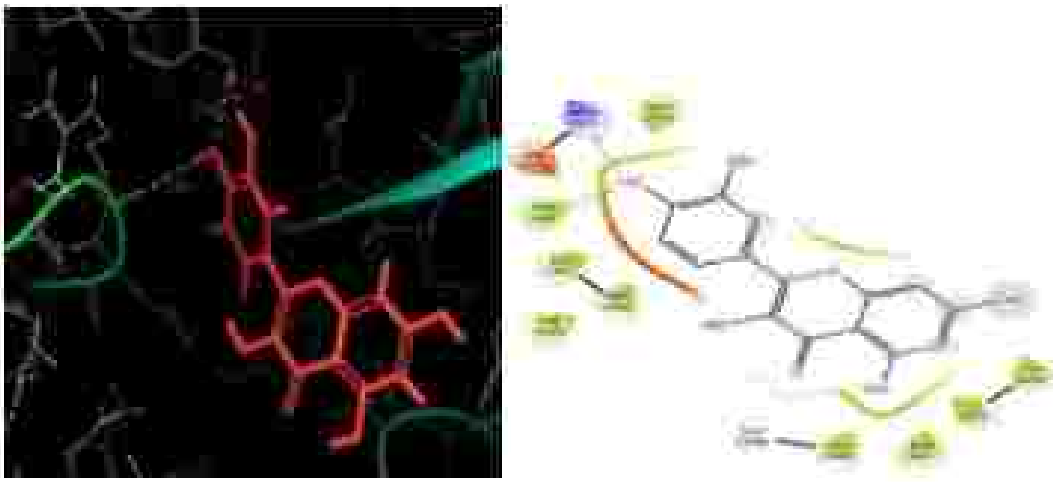

Figure 36. 3D and 2D Structure of Quercetin (KDR)

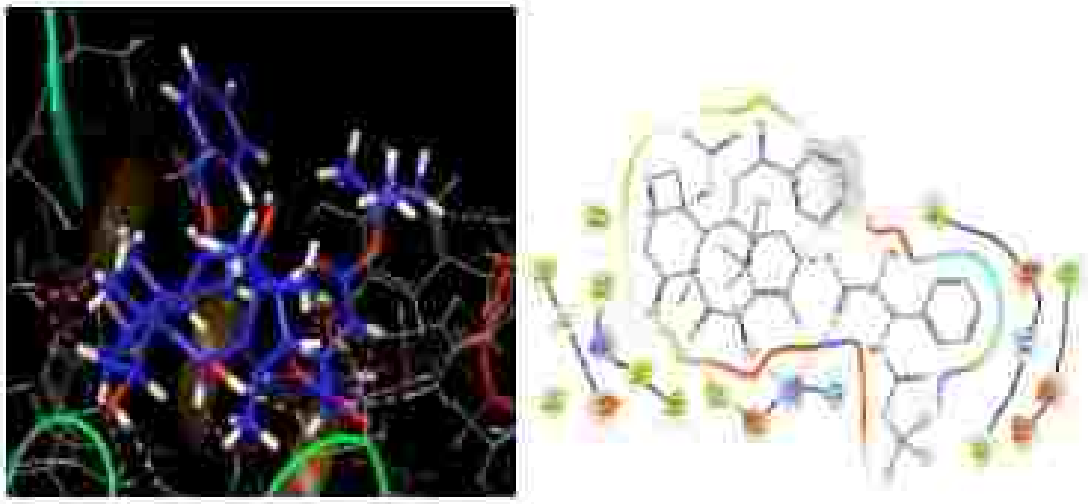

Figure 36. a. 3D and 2D Structure of Docetaxel

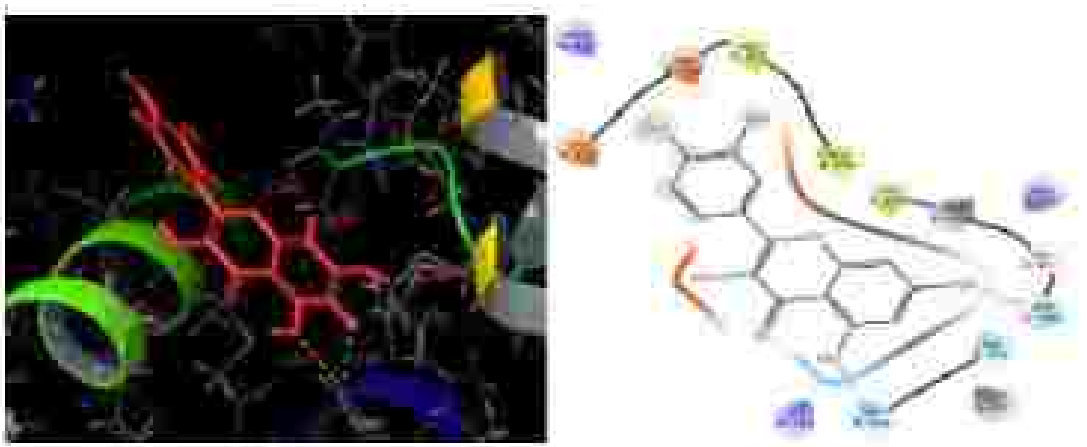

Figure 37. 3D and 2D Structure of Quercetin (ESR1)

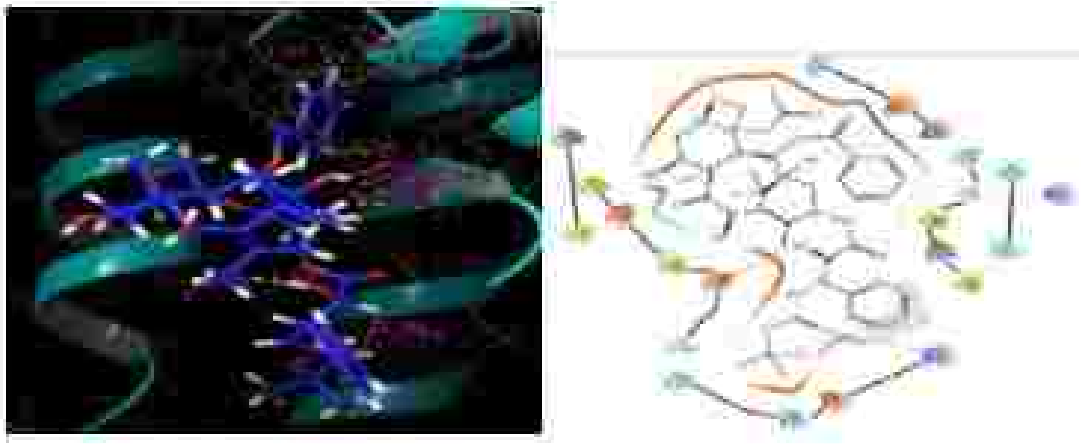

Figure 37. a. 3D and 2D Structure of Docetaxel

The molecular docking results revealed that among the ligands tested against MMP9 (PDB ID: 1L3D), quercetin exhibited the highest binding affinity with a docking score of -8.68 kcal/mol, which is significantly stronger than that of the standard drug- docetaxel (-5.318 kcal/mol). This suggests that quercetin may have a stronger interaction with MMP9, offering better inhibition potential. Other ligands such as gamma-sitosterol (-4.53 kcal/mol), beta-sitosterol (-4.56 kcal/mol) and 2,3,4,6-tetramethoxystyrene (-4.23 kcal/mol) showed moderate affinities, while alpha-amyrin had the weakest binding affinity (-3.56 kcal/mol) still comparable to docetaxel. For EGFR (PDB ID: 6S9B), quercetin again demonstrated the strongest binding affinity at -6.40 kcal/mol, outperforming docetaxel (-3.783 kcal/mol). The other ligands including 2,3,4,6-tetramethoxystyrene (-3.29 kcal/mol), beta-sitosterol (-2.67 kcal/mol) and gamma-sitosterol (-1.31 kcal/mol) showed weaker interactions with alpha-amyrin having the lowest score (-1.16 kcal/mol).

For KDR (PDB ID: 6GQG) quercetin maintained a high binding score of -6.05 kcal/mol, which is comparable to docetaxel (-6.621 kcal/mol) while other ligands including gamma-sitosterol (-3.05 kcal/mol), beta-sitosterol (-3.04 kcal/mol) and alpha-amyrin (-3.01 kcal/mol) displayed considerably

lower affinities. For the ESR1 (PDB ID: 1ERR) quercetin once again demonstrated the highest binding affinity (-5.37 kcal/mol) slightly lower than docetaxel (-5.698 kcal/mol). Other ligands such as 2,3',4,6-tetramethoxystyrene (-3.28 kcal/mol), beta-sitosterol (-3.05 kcal/mol) and alpha-amyrin (-2.62 kcal/mol) showed moderate binding, while gamma-sitosterol exhibited the lowest affinity (-2.52 kcal/mol). These findings suggest that quercetin with consistently higher binding affinities across all targets compared to docetaxel, holds potential as a stronger anticancer agent particularly in inhibiting proteins such as MMP9 and EGFR.

4.20. Molecular Dynamics Simulation (MDs)

Molecular dynamics simulations (MDs) are used to predict the stability of protein-ligand complexes under various physiological conditions including changes in pressure, temperature and the presence of water molecules. In this study, MD simulations were performed over approximately 100 ns.

4.20.1. Root Mean Square Deviation (RMSD)

The RMSD graph displays the stability and conformational changes of both the protein and the ligand throughout the formation of their complex (Figure. 38). RMSD values typically indicate the binding energy and interactions between the protein and ligand. In the graph, protein stability is shown in blue, while ligand stability is represented in red (Figure. 38). The analysis of RMSD values across different protein-ligand complexes reveals distinct fluctuation and stabilization patterns. For the complex 1B3D, the first fluctuation occurred at 13.10 ns, with protein RMSD at 2.47 Å and ligand RMSD at 1.53 Å. In contrast, 6S9B exhibited an initial fluctuation at 4.00 ns, showing higher RMSD values for both protein (2.77 Å), ligand (4.14 Å) and later stabilized at 14.10 ns with increased RMSD values (protein at 3.68 Å, ligand at 6.16 Å). The 6GQ0 complex initially fluctuated at 4.30 ns, with a significantly high ligand RMSD of 13.32 Å but stabilized by 40.50 ns, reducing ligand RMSD to 5.54 Å while protein RMSD remained relatively stable at 2.05 Å. For 1ERR, fluctuations were observed first at 3.40 ns with RMSD values of 1.81 Å for the protein and 6.40 Å for the ligand, followed by stabilization at 9.90 ns (protein RMSD: 2.21 Å, ligand RMSD: 6.67 Å) and a subsequent

fluctuation at 63.80 ns, where the protein RMSD increased to 3.23 Å and ligand RMSD decreased to 4.49 Å. These fluctuations could be attributed to changes in the ligand's conformation.

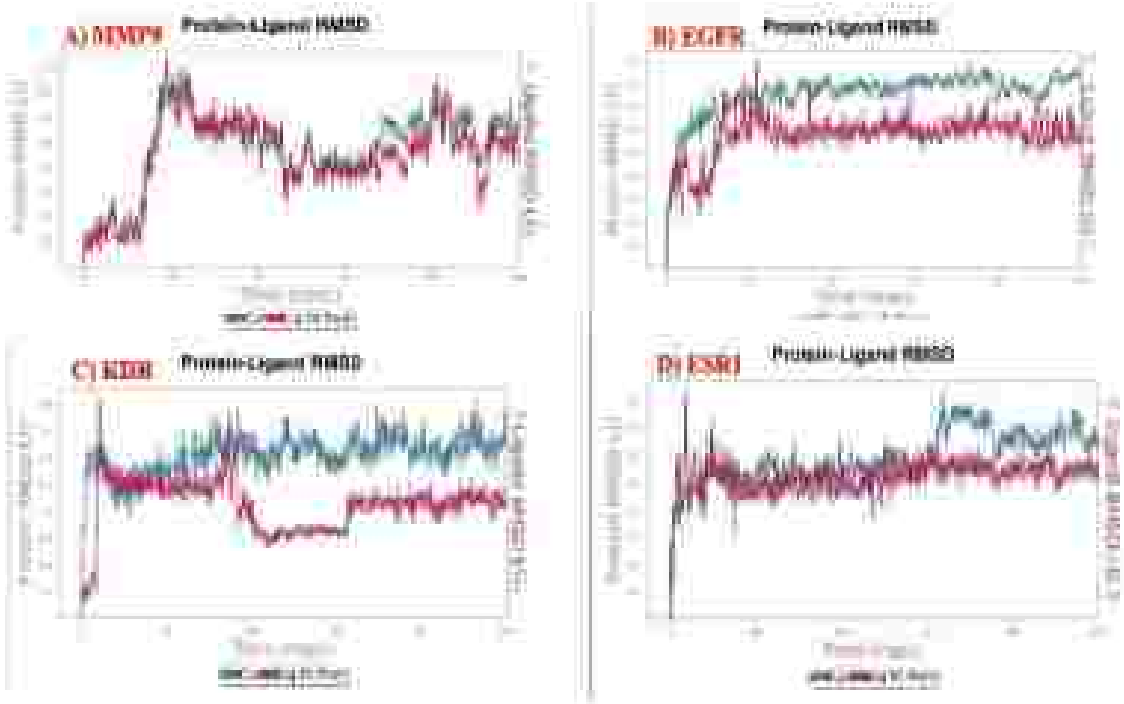

Figure 38. Illustration Of RMSD, the Stability of the Protein (Depicted in Blue) and the Ligand (Depicted in Red) within the Complex.

4.20.2. Root Mean Square Fluctuation (RMSF)

Root Mean Square Fluctuations (RMSF) are employed to assess the transient structural changes in both the protein (P-RMSF) and the ligand (L-RMSF) throughout the simulation. RMSF provides insights into the flexibility of the protein structure during interactions(Figure 39).

For Chain A in one dataset, the C-alpha atoms exhibit varying degrees of flexibility with measurements such as 3.92 Å at residue 197 (GLU) and a range of values for other residues including 1.57 Å at residue 201 (HIS) and up to 4.91 Å at residue 225 (SER). Similarly, Chain B shows fluctuations from 2.77 Å at residue 234 (LEU) to 4.19 Å at residue 194 (ASN). Another dataset reveals Chain A with minimal flexibility such as 0.39 Å at residue 1046 (ASP) and up to 1.86 Å at residue 459 (NMA) with further variability noted at residues like 0.71 Å at residue 884 (SER) and 1.50 Å at residue 1064 (ASP). Additionally, Chain A in a third dataset displays a range from 0.56 Å at residue

445 (ASN) to 3.16 Å at residue 470 (GLU) while Chain B presents values such as 1.35 Å at residue 411 (ASP) and the lowest at 0.79 Å for residue 430 (ALA). This comprehensive analysis across different chains and datasets highlights the dynamic behaviour and variability in the flexibility of the protein's structure throughout the simulation.

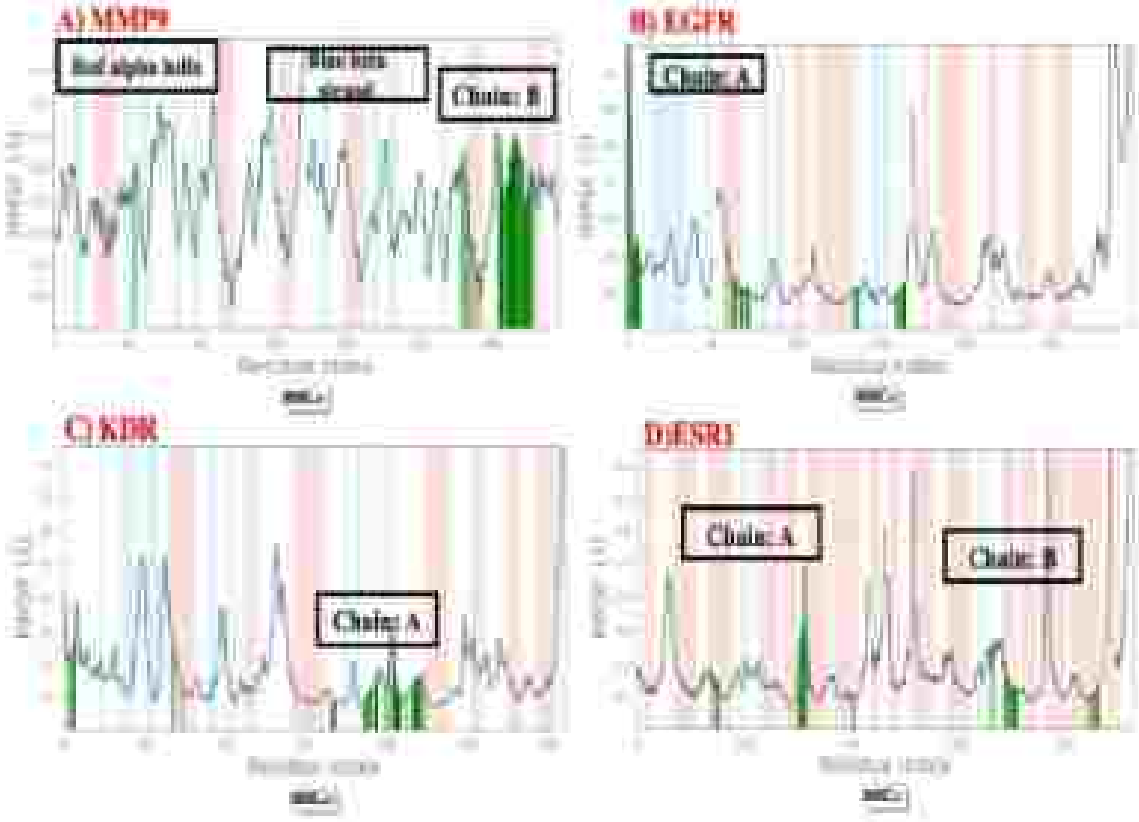

Figure 39. Illustration of RMSF Plot for Quercetin, with the following PDB Ids: A- MMP9, B- EGFR, C- KDR, D- ESR1.

4.20.3. Ligand Properties:

The properties of the ligand Quercetin such as radius of gyration (rGyr), RMSD, intramolecular hydrogen bonds (intraHB), molecular surface area (MolSA), solvent accessible surface area (SASA) and polar surface area (PSA) are within optimal ranges and are consistent with those observed for other substrates and co-crystal ligands. This suggests that Quercetin is well-suited for drug discovery. Solvent Accessible Surface Area (SASA) measures the surface area of a biomolecule that is accessible to solvent. This metric is critical for evaluating the free energy needed to transfer a biomolecule

from an aqueous environment to a non-polar environment such as a lipid bilayer. An optimal SASA is essential for facilitating efficient movement toward the binding pocket. Additionally, Quercetin established intramolecular hydrogen bonds with the 1B3D protein. During the simulation, Quercetin's molecular surface area (MolSA) and polar surface area (PSA) remained stable up to 100 ns, while other parameters exhibited fluctuations throughout the entire duration. For the 6S9B protein, only the RMSD and SASA showed fluctuations at 10 ns but stabilized for the rest of the 100 ns simulation.

In the case of the 6GQ0 protein, RMSD and SASA fluctuated at 31 ns, stabilized by 44 ns then fluctuated again at 88 ns before stabilizing until the end of the simulation at 100 ns. The other parameters were stable throughout the 100 ns simulation. For the 1ERR protein, RMSD and SASA showed fluctuations at 0.60 ns, stabilized by 6.90 ns, then fluctuated again at 87 ns before achieving stability at 91 ns. All other parameters remained stable throughout the entire 100 ns simulation.

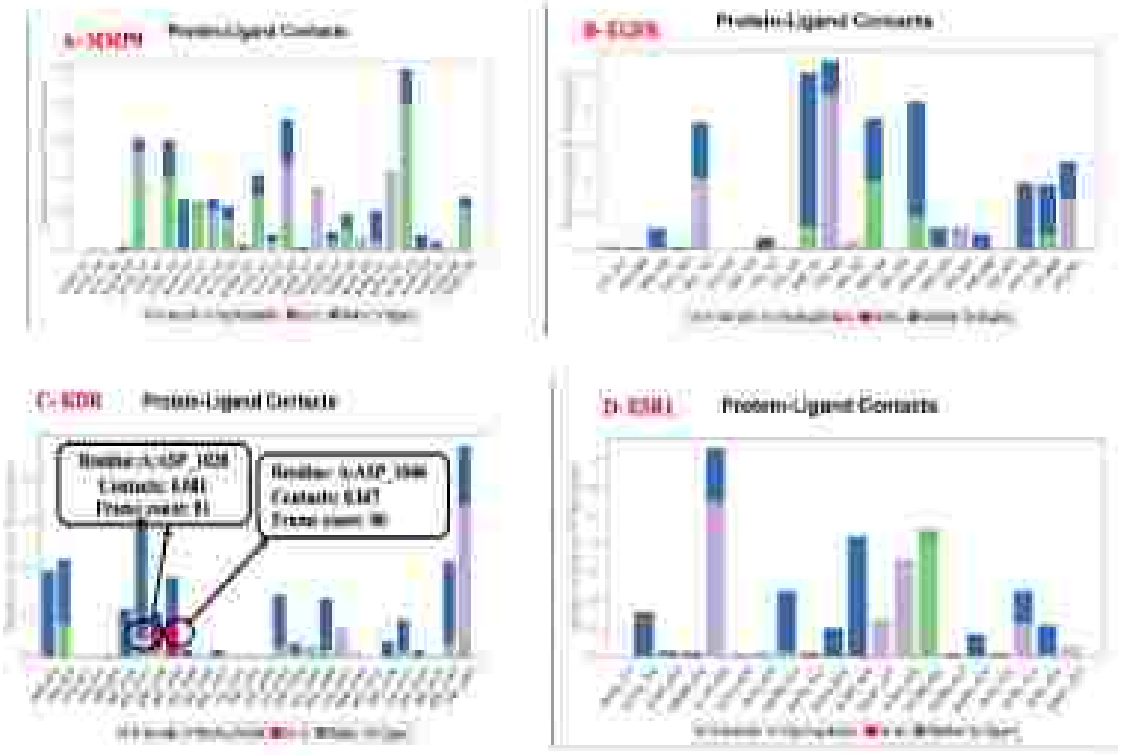

Figure 40. Protein-Ligands Contacts- The Bar Graph of Proteins (MMP9, EGFR, KDR and ESR1) with Quercetin

Molecular Dynamics (MDs) simulation is a computational method that models the physical motions of atoms and molecules over time with classical mechanics principles. Thereby, this approach allows one to observe the dynamic behaviour of molecular systems at the atomic level and gain insights into further the structural, functional properties of complex biological systems such as proteins, lipids and nucleic acids (Filipe & Loura, 2022). MD simulation techniques aid understanding of molecular interactions, membrane permeability, protein-ligand binding and drug mechanisms. The applications are extended to the characterization of biomolecular systems, to aid experimental design and to predict properties of chemical systems nearly inaccessible to experimentalist determination.

Molecular Dynamics simulations provide a really powerful tool to be either used for solid fundamental research or for finding practical applications pushing forward the advancement of biochemistry, pharmacology and materials science. Yang *et al*, 2022 found that quercetin complexes manifested stable binding in molecular dynamics simulations, which was also confirmed by compatible results from molecular docking. Stability originated from dynamic interactions such as *Van der Waals* forces, electrostatic interactions and hydrogen bonding, thereby suggesting that quercetin could be an interesting molecule capable of modulation of gastric cancer pathogenesis through these target proteins. In this study, however, attention is focused on quercetin in isolation for dynamic simulation, quercetin having the most potent binding energy among all the tested compounds. Simulations performed with PDB ID-6S9B showed stable results against those of PDB ID-1B3D, 6GQ9 and 1ERR.

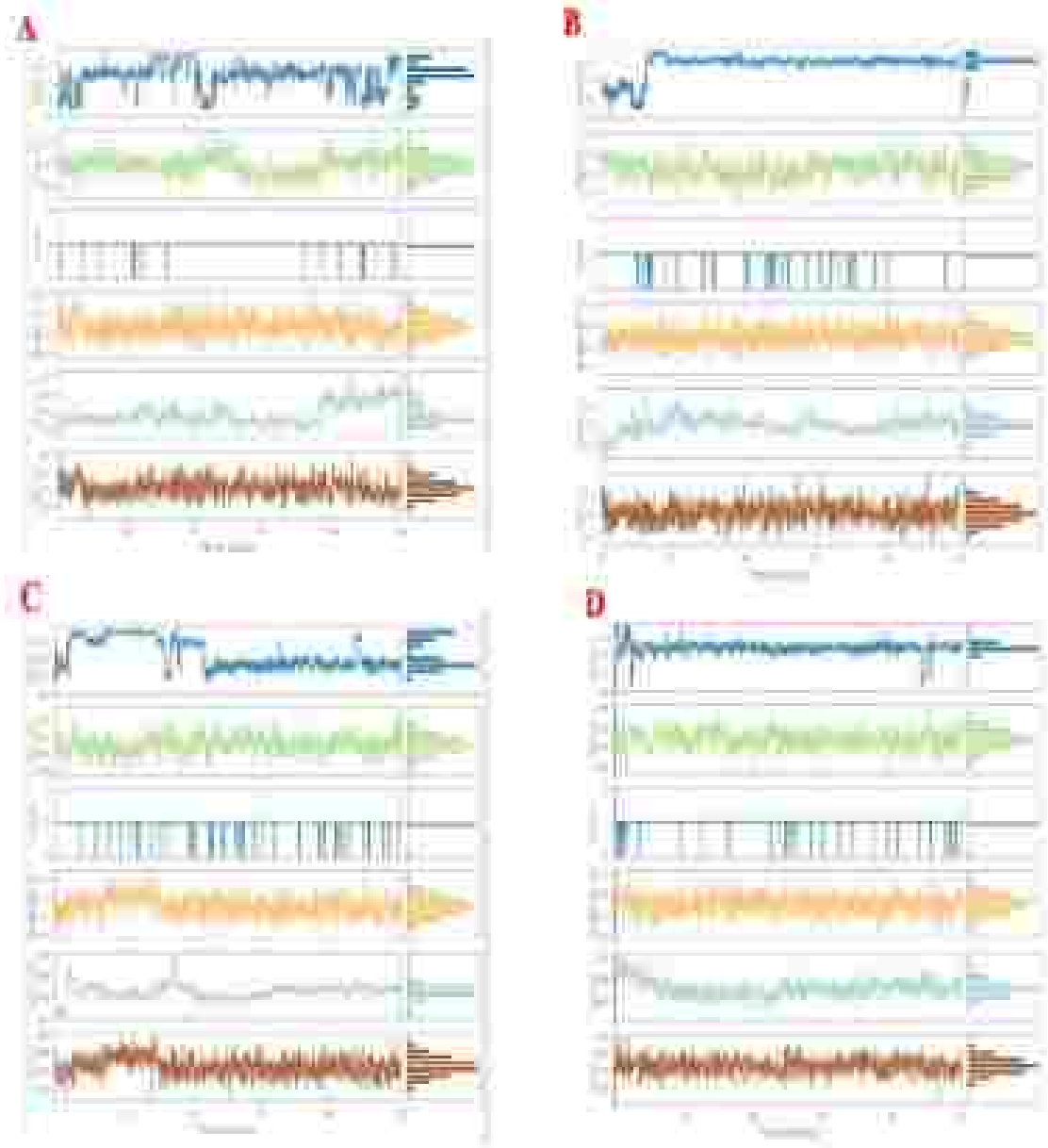

Figure 41. The Ligand Properties Of Quercetin, encompass the Radius of Gyration (Rgyr), Intramolecular Hydrogen Bonding (Intrahb), Molecular Surface Area (Molsa), Solvent Accessible Surface Area (SASA) and Polar Surface Area (PSA).